Texas A&M University
Mechanical Engineering Department
Turbomachinery Laboratory
Tribology Group

LEAKAGE AND ROTORDYNAMIC FORCE COEFFICIENTS OF A THREE-WAVE (AIR IN OIL) WET ANNULAR SEAL: MEASUREMENTS AND PREDICTIONS

Research Progress Report to the Turbomachinery Research Consortium

TRC-SEAL-01-17

by

Xueliang Lu
Research Assistant

Luis San Andrés
Mast-Childs Chair Professor
Principal Investigator

May 2017

***WET* (BUBBLY) SEALS FOR SUB-SEA MULTIPLE PHASE PUMPS AND *WET* COMPRESSORS**
TRC Project, TEES # 400124-00079

EXECUTIVE SUMMARY

In the subsea oil and gas industry, multiphase pumps and wet gas compressors add pressure to the process fluid thus enabling long distance a tie back system that eliminates topside facilities such as an oil and gas separation stations. One challenge to construct a reliable multiphase pump or a wet gas compressor is to engineer their ability to withstand a gas-liquid mixture whose gas volume fraction (GVF) or liquid volume fraction (LVF) changes over time. The mixture GVF or LVF affects the static and dynamic forced performance of secondary flow components, namely seals, and which may lead to an increase in both rotor lateral or axial vibrations.

The reports presents measurements of leakage and dynamic force coefficients for a three-wave seal (L = 46 mm, D = 127 mm, c_m = 0.191 mm). The wavy-seal should deliver a significant centering stiffness, as opposed to that from a uniform clearance seal. At a shaft speed of 3.5 krpm, an air in ISO VG 10 oil mixture with an inlet GVF varying discretely from 0 to 0.9 feeds the seal at a supply pressure P_s of 2.5 bar(a). The test mixture mass flow rate decreases continuously with an increase in inlet GVF. The seal with pure liquid (GVF=0) shows frequency independent force coefficients. On the other hand, operation with a mixture gives stiffness coefficients that vary greatly with frequency, in particular the direct stiffness that hardens. The direct damping coefficients, on the other hand, are not functions of excitation frequency, albeit dropping rapidly in magnitude as the GVF increases.

The report also presents comparison of force coefficients for three seals: a three-wave seal and two plain annular seals: one with the same mean clearance as the three-wave seal, and the other with a clearance equal to the maximum clearance of the wavy-seal. This last seal emulates a worn surface condition. The three-wave seal produces the greatest direct stiffness and damping, as well as the largest effective damping coefficient. The worn surface seal produces the smallest force coefficients and leaks the most.

Predictions of three-wave seal force coefficients derived from a homogeneous bulk flow match well with the test data for operation with a pure oil and an inlet GVF 0.2. The discrepancy between the prediction and experimental data grows rapidly for operation with a larger gas content, GVF > 0.2.

Table of Contents

List of Tables

List of Figures

Introduction

In the subsea oil and gas industry, multiphase pumping and wet gas compression systems help to add pressure to well effluents, thus extending the life of depleting wells to increase oil recovery. The increase in pressure of crude oil also enables long distance tieback systems to reduce cost associated with top surface facilities [1]. Future subsea compressors will feature a 50% reduce in size and weight to lower capital investment without compromising availability [2,3]. One challenge for multiphase processing is that wet gas compressors have to work with up to a 5% liquid volume fraction [4,5] and multiphase pumps need to handle a gas-liquid mixture with up to 100% gas [1]. A variation in mixture gas volume fraction (GVF) changes the fluid physical properties, namely density (compressibility) and viscosity, as compared with a single phase component.

Secondary flow components operating with liquid-gas (two-component) mixtures are known to cause rotordynamic instability issues in centrifugal compressors, as learnt since 1972 when a field test showed that the injection of liquid into a *shaft-end* labyrinth seal in a back to back multistage compressor caused significant rotor sub-synchronous lateral vibrations (~0.5X) [5]. Later in 1993, Iwatsubo and Nishino [6] report test results in a pump annular seal operating with an air in water mixture. The authors find a steady decrease in rotordynamic force coefficients when the GVF increases, and a high amplitude random rotor lateral vibration occurring for tests with GVF > 0.7.

Interest on wet annular seals has grown rapidly since 2005 when a single stage compressor operating with a mixture of natural gas and a hydrocarbon liquid was tested in Norway [7]. Severe sub-synchronous vibration (SSV) with 50% whirl speed appeared when the inlet liquid volume fraction (LVF) increased above 3%. The authors suspect the trapped liquid in the seal cavities caused a system rotordynamic instability.

Later in 2014, Vannini et al. [5] find a rotor SSV at 0.45X in a compressor equipped with labyrinth seals for operation with just 0.5% LVF. However, typical design for a wet gas compressor calls for LVF as high as 5% [4,5]. Vannini et al. [8] in 2016 conduct Computational Fluid Dynamics (CFD) analysis to study the flow field in a labyrinth seal and in a pocket damper seal. The analysis uses an Euler-Euler-VOF[1] method to model the

[1] The model assumes an inhomogeneous mixture whose components share the pressure field but have different velocity fields.

multiphase flow. The results demonstrate a quick accumulation (pooling) of liquid in the first cavity of the labyrinth seal, and which extends to the downstream cavities as time elapses. The trapped liquid circulates along the seal circumference direction with significant momentum. A pocket damper seal (PDS), however, appears not to entrap the liquid. Indeed, a test campaign in Ref. [5] demonstrates that a PDS produced a rotor dynamically stable compressor even with a significant wet gas condition.

The presence of liquid in a gas stream is also found to cause rotor axial vibrations in centrifugal compressors. During a performance test for a two stage wet gas centrifugal compressor, Ransom et al. [9] (2011) document rotor axial vibrations at a low frequency (0.5 Hz) which evolve into a broad band motion (10 -15 Hz) as the LVF increases. The low frequency axial motion disappears when the water injection into the main gas stream stops. The authors postulate that a change in the liquid volume fraction (LVF) of the wet gas produces a change in the thrust load at the location of the balance piston seal, thus inducing the rotor axial vibrations.

The noted problems related to annular wet seals in multiphase pumps and wet gas compressors promote further research in such seals operating with gas and liquid (controlled) mixtures. San Andrés [10] (2010) develops a bulk-flow model (BFM) to predict the static and dynamic forced performance of textured seals operating with a homogeneous two-component flow mixture. Predictions show the seal leakage, direct damping and power loss decrease steadily with an increase in inlet GVF. The seal force coefficients also decrease rapidly with excitation frequency if the mixture has a large GVF. Arghir et al. [11] (2011), also using a BFM, predict the rotordynamic force coefficients in a textured annular seal operating with an air in water bubbly flow. The authors note that changes in GVF from 1% to 10% can produce frequency dependent force coefficients.

San Andrés et al. [12] (2016) present measurements conducted in a (non-rotating) short length (L/D = 0.36) annular seal supplied with an air in oil (ISO VG10) mixture and report that an increase in the liquid volume fraction (LVF) in an otherwise pure gas leads to a higher leakage, and dramatically increases its damping coefficients. In tests with pure air and also with a mixture with liquid content at LVF= 2% and 4%, both under a pressure supply/pressure discharge ratio = 2.0, the test results in Ref. [12] reveal a small amount of liquid increases ten-fold (or more) the damping coefficients of the wet seal.

Voigt et al. [13] (2016) detail the design of a large test facility to perform dynamic load tests to annular seals supplied with a wet gas with LVF to 5%, or a bubbly mixture with air content to 5%. The test rig whose rotor is supported on two active magnetic bearings can run up to 10 krpm and reach a maximum supply pressure of 65 bar. Using CFD, Voigt et al. [14] (2016) predict the rotordynamic force coefficients of a smooth surface annular seal (L/D = 0.75) operating with a water in air (wet gas) or air in water (bubbly mixture) mixture. For a wet gas, an increase in LVF to 5% produces an increase in direct stiffness and damping coefficients. For operation with GVF < 5%, the predictions show a dramatic increase in direct damping with frequency and no added mass effect. Even for operation with a pure liquid, the authors report a dynamic stiffness that decreases linearly with frequency, which points to an error as a liquid seal (with GVF = 0) evidences considerable fluid inertia effects [15,16].

San Andrés and Lu [17] (2017) present extensive experimental work and analysis on the static and dynamic performance of a short length (L/D = 0.36), smooth surface annular seal lubricated with an air in ISO VG10 oil mixture with inlet GVF increasing discretely from 0 to 0.9. The test are conducted at a supply pressure (P_s) up to 3.5 bar(a), discharge pressure (P_a) = 1 bar(a), and various shaft speed (Ω) to 3.5 krpm (ΩR = 23.3 m/s). For operation with either with a pure oil or an air in oil mixture the flow is laminar. The seal leakage and drag power decrease monotonically by 25% and 85% respectively as the mixture inlet GVF increases from 0 (pure oil) to 0.9. For operation with supply pressure P_s = 2.5 bar(a) and rotor speed equal to 3.5 krpm, the seal lubricated with a pure liquid produces a frequency independent direct stiffness (K), added mass (M) and viscous damping (C). For tests with a mixture (GVF_{max} = 0.9), the seal dynamic complex dynamic stiffness Re(H) increases (hardening) with whirl frequency (ω). Both the seal cross coupled stiffnesses (K_{XY} and $-K_{YX}$) and direct damping (C_{XX} and C_{YY}) coefficients decrease by approximately 75% as the inlet GVF increases to 0.9. The cross-over frequency at which the effective damping coefficient $C_{XXeff} = C_{XX} - K_{XY}/\omega \rightarrow 0$ drops from 50% of rotor speed (ω = ½ Ω) for a liquid seal to a lesser magnitude for operation with an air/oil mixture. Predictions for leakage and drag power based on a homogeneous bulk flow model match well with the test data for operation with inlet GVF up to 0.9. Predicted force coefficients correlate well with the test data for mixtures with GVF up to 0.6. For a mixture with a

larger GVF, the model under predicts the direct damping coefficients by as much as 40%. The tests also reveal the appearance of a self-excited seal motion with a low frequency; its amplitude and broad band frequency (centered at around ~12 Hz) persist and increase as the gas content in the mixture increase.

Zhang et al. [18] (2017) present test results for leakage and rotordynamic force coefficients obtained with a long, smooth annular seal (D = 89.3 mm, L/D = 0.65, and c = 0.188 mm) operating with an air in silicon oil (PSF-5cSt) mixture with LVF $\leq$ 8%, at a supply pressure of 62.1 bar and at a top shaft speed 20 krpm (ΩR = 93.5 m/s). The authors report a ~5% decrease in mass flow rate as the LVF increases from 0 to 2%, which later increases by ~50% as the LVF further increases to 8%. For operation with discharge pressure/supply pressure ratio = 0.5 and 0.57 and at a shaft speed from 10 krpm to 20 krpm, the seal direct dynamic stiffness (K) decreases continuously as the inlet LVF increases from 0 to 8%. The cross coupled stiffnesses (k) increase two to three times, depending on shaft speed. When lubricated with either a pure air or a mixture, both K and k increase with excitation frequency. The tests show constant viscous direct (C) and cross coupled damping coefficients (c) for operation with either a pure air or a mixture. That is, damping coefficients are not a function of frequency. The authors report a continuous increase in damping (C) as the inlet LVF increases from 0 to 8%. An increase in the inlet LVF of a wet gas causes an increase in the cross-over frequency where $C_{eff} \rightarrow 0$.

The reviewed literature demonstrates that annular seals are important to the rotordynamics of wet gas centrifugal compressors. Vannini et al. [8] demonstrate that a pocket damper seal is a viable solution for wet gas compressors. However, besides three publications by Iwatsubo and Nishino [6] in 1993, San Andrés and Lu [17] and Zhang et al. [18] in 2017, there is scant literature relevant to seals operating with bubbly mixtures. Thus, there is a need to find/test proven seal types for multiphase pumps and wet gas compressors.

The search for seal configurations with notable characteristics calls for seal types with textured surfaces (damper seals), helical grooved seals, etc. Leader et al. [19] successfully reduce SSV in a vertical liquid sulfur pump (single phase flow) by replacing plain cylindrical bearings with a three-lobe profile bearing design. Leader claims that a lobular seal produces a larger direct stiffness than a plain bearing does, thus raising the pump

critical speed above its operating speed, and which delays the onset of instability to a higher rotor speed.

For gas machinery applications, Dimofte [20] in 1994 introduce s wavy-surface journal bearing (akin to a multiple lobe bearing) with improved stability due to its centering stiffness generated by a (built-in) mechanical preload. Dimofte [21], Dimofte and Hendricks [22], and Ene et al. [23] later demonstrate wavy-surface journal bearings are effective to enhance stability for operation with either gas or liquid lubricants. However, this simple bearing configuration is yet to be tested as a seal or with a mixture of gas in liquid. A seal with a lobular shape, elliptical in particular, can be attained in practice by simply crushing the bushing when installed in a pump.

This report discusses the experimental and predicted static and dynamic forced performance of a three-wave seal with a diameter D = 127 mm, length L = 46 mm (L/D = 0.36), and mean clearance c_m = 0.191 mm. In tests with the shaft spinning at an angular speed of 3.5 krpm (58.3 Hz, ΩR = 23.3 m/s), an air in ISO VG10 oil mixture with inlet GVF from 0 to 0.9 feeds the seal at a supply pressure of 2.5 bar(a). Dynamic loads with frequency = 20 Hz to 150 Hz exerted on the seal housing aim to produce data to extract the seal force coefficients.

The report also presents comparisons of the static and dynamic performance of a three-wave seal against that of a plain cylindrical annular seal [17] having the same length and diameter and operating under the same conditions. The three-wave seal has a mean clearance (c = 0.191 mm) equal to that of the plain annular seal. Test results show that the three-wave seal produces larger direct stiffness, direct damping and effective damping coefficients for operation with either a pure oil or a mixture.

Eventually, a pump will wear out and the wavy features in the (three-wave) seal surface will disappear to produce a higher leakage and alter its force coefficients. To simulate a seal worn condition the report also shows test results of a cylindrical annular seal with a clearance equal in size to the maximum clearance of the three-wave seal (c_{max} = 0.274 mm).

Test rig description

Figure 1 depicts the geometry of a three-wave seal and Table 1 lists the dimensions of the seal and the fluids physical properties. The test seal has a diameter D = 127 mm and length L = 46 mm. For operation with a load (W) in line with the $+X$ axis and with the rotor spinning at an angular speed Ω, the film thickness between the outer surface of the rotor and the inner surface of the seal element follows [23]:

$$h = c_m + e_X \cos(\Theta) + e_Y \sin(\Theta) + e_w \cos\left(n_w (\Theta - \gamma)\right) \quad (1)$$

where Θ = 0° to 360° is a circumferential angle starting from the $-X$ axis, c_m is a mean clearance, e is the rotor eccentricity, $e_w = c_{max} - c_m$ is the wave amplitude, n_w is the number of wave, and α is the angle between the line of start of a wave and the line connecting the center of the rotor and the seal. γ is the angle between the start point of a wave and the direction of the applied load. At a journal centered condition, W = 0, and α =0°.

Figure 2 shows the design and measured clearance profile for the three-wave seal. The test seal has a maximum clearance c_{max} = 0.274 ± 0.002 mm, a minimum clearance c_{min} = 0.108 ± 0.002 mm, a mean clearance c_m = ½(c_{min} + c_{max}) = 0.191 ± 0.004 mm, and a wave amplitude $e_w = c_{min} - c_m$ = 0.083 ± 0.004 mm. Note the wave amplitude ratio $\varepsilon_w = e_w/c_m$ = 0.43.

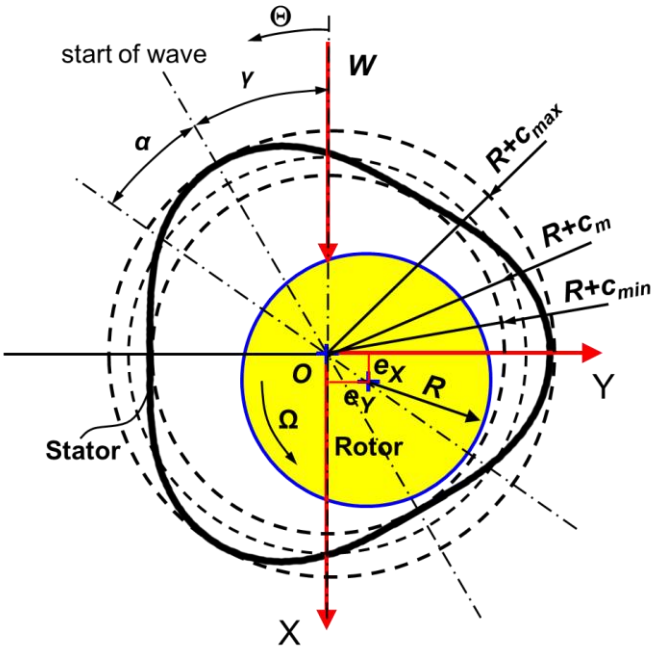

Fig. 1 Geometry of a three-wave annular seal. L = 46 mm, D = 127 mm, c_{max} = 0.274 mm, c_{min} = 0.108 mm, c_m = 0.191 mm, e_w = 0.083 mm, n_w = 3.

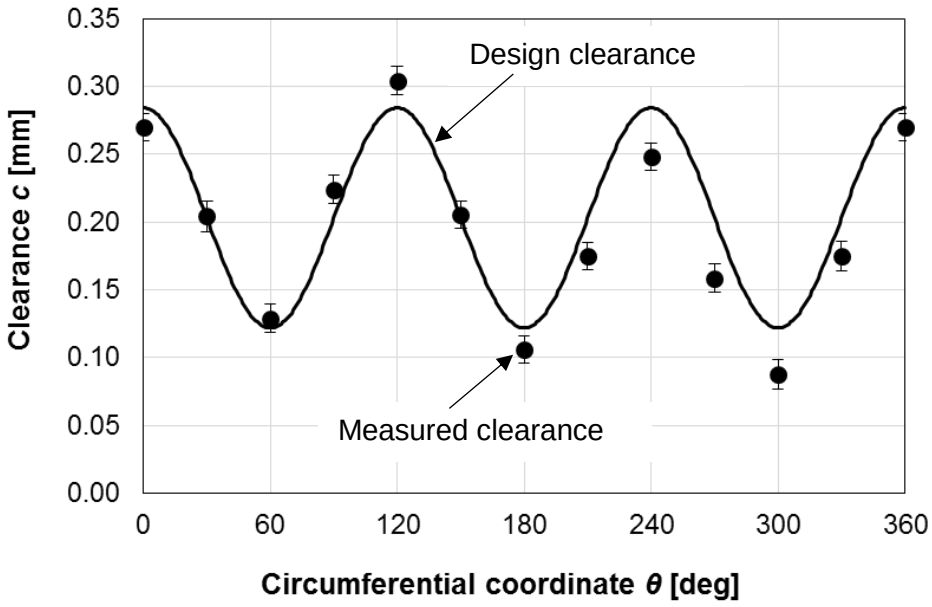

Line: design clearance, symbol: measured clearance

Fig. 2 Design and measured clearance profile of three-wave seal. L= 46 mm, D = 127 mm, c_{max} = 0.274 mm, c_{min} = 0.108 mm, c_m = 0.191 mm, e_w = 0.083 mm, n_w = 3.

Table 1. Dimensions of three-wave annular seal and fluids physical properties.

Diameter, $D = 2R$	127 mm
Length, L	46 mm
Number of waves	3
Maximum radial clearance, c_{max}	0.274± 0.002 mm
Minimum radial clearance, c_{min}	0.108± 0.002 mm
Mean radial Clearance, $c_m = ½(c_{min} + c_{max})$	0.191 ± 0.004 mm
Wave amplitude, $e_w = c_{min} - c_m$	0.083 mm, $\varepsilon_w = e_w/c_m$ =0.43
ISO VG10 viscosity, μ_l	10.1 cP (at 37 ºC)
Density, ρ_l	830 kg/m^3
Air viscosity, μ_{ga}	0.019 cP (at 37 ºC)
Density, ρ_{ga}	1.14 kg/m^3 at P_a = 1 bar(a)
Max test supply & discharge pressures	3.5 bar(a), 1 bar(a)
Top journal speed, Ω_{max}	3.5 krpm
Rotor surface speed, $½D\Omega_{max}$	23.3 m/s

Figure 3 shows a 3-D isometric view of the seal test rig and the coordinate system (X, Y) for reference of the seal motion. The test rig is modified from an earlier test rig described in Ref. [17]. Four flexible support rods (90° apart) with a total lateral stiffness K_s and structural damping coefficient C_s connect the seal housing to a massive steel base. Two electromagnetic shakers with a load capacity of 440 N ± 9 N (100 lb$_f$), and installed 90°

(*X*, *Y*) apart, can excite the seal assembly via two long stingers to produce dynamic motions for the identification of force coefficients. The long stingers are designed according to the procedure advanced by Mitchell and Elliott [24] to isolate the test seal from the two shakers. That is, the shakers do not constraint the lateral motion of the seal housing during a test. The test rig is designed such that the mass center of the assembled seal housing in the horizontal plane is in line with the axes (*X*, *Y*) of the stingers.

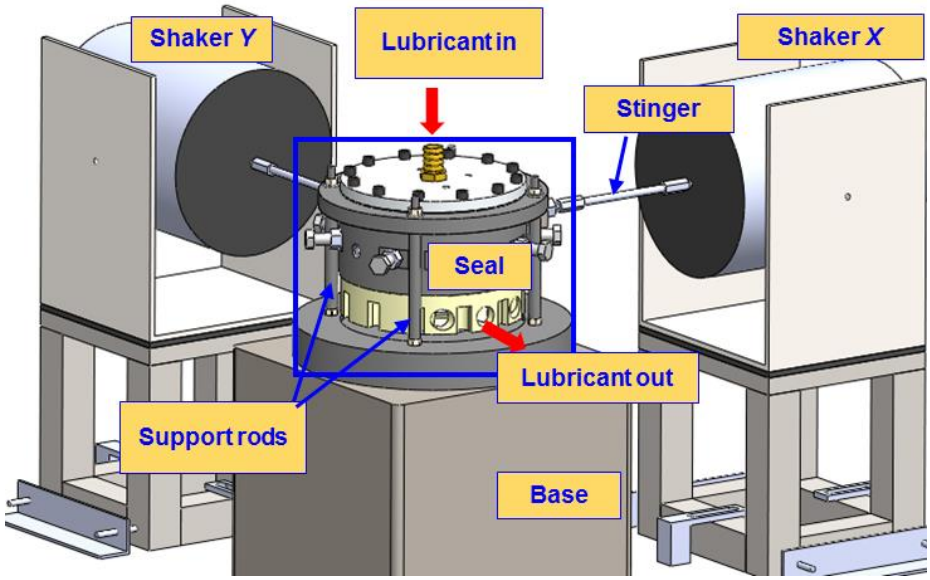

Fig. 3 Isometric view of seal test rig with shakers and lubricant supply line

Figure 4(a) shows a cross section view of the seal assembly with the lubricant flow path. The narrow gap between the ID of a test element and the OD of a rotating journal makes the lubricant sealing section. A DC motor, through a transmission belt with a gear ratio of 1.8, drives the shaft and journal. This shaft is supported on two rigid ball bearings (the graph only shows a top ball bearing) and can spin to a maximum speed of 6 krpm

The arrangement allows to exchange a test seal element without disassembling the entire mechanical structure. A seal element is installed inside a housing whose inner diameter (ID) is 3 mm larger than the outside diameter (OD) of the seal. Figure 4(b), cross section A-A, details the seal installation inside the casing. Four sets (2 bolts each) of centering bolts, 20˚ apart, inserted in the housing allow radial adjustment of the seal element. During the centering process, a feeler gauge measures the clearance (*c*) between

the journal and the seal. After the seal is centered, a top lid with a bottom surface contacting the top surface of the seal element presses it against the seal housing.

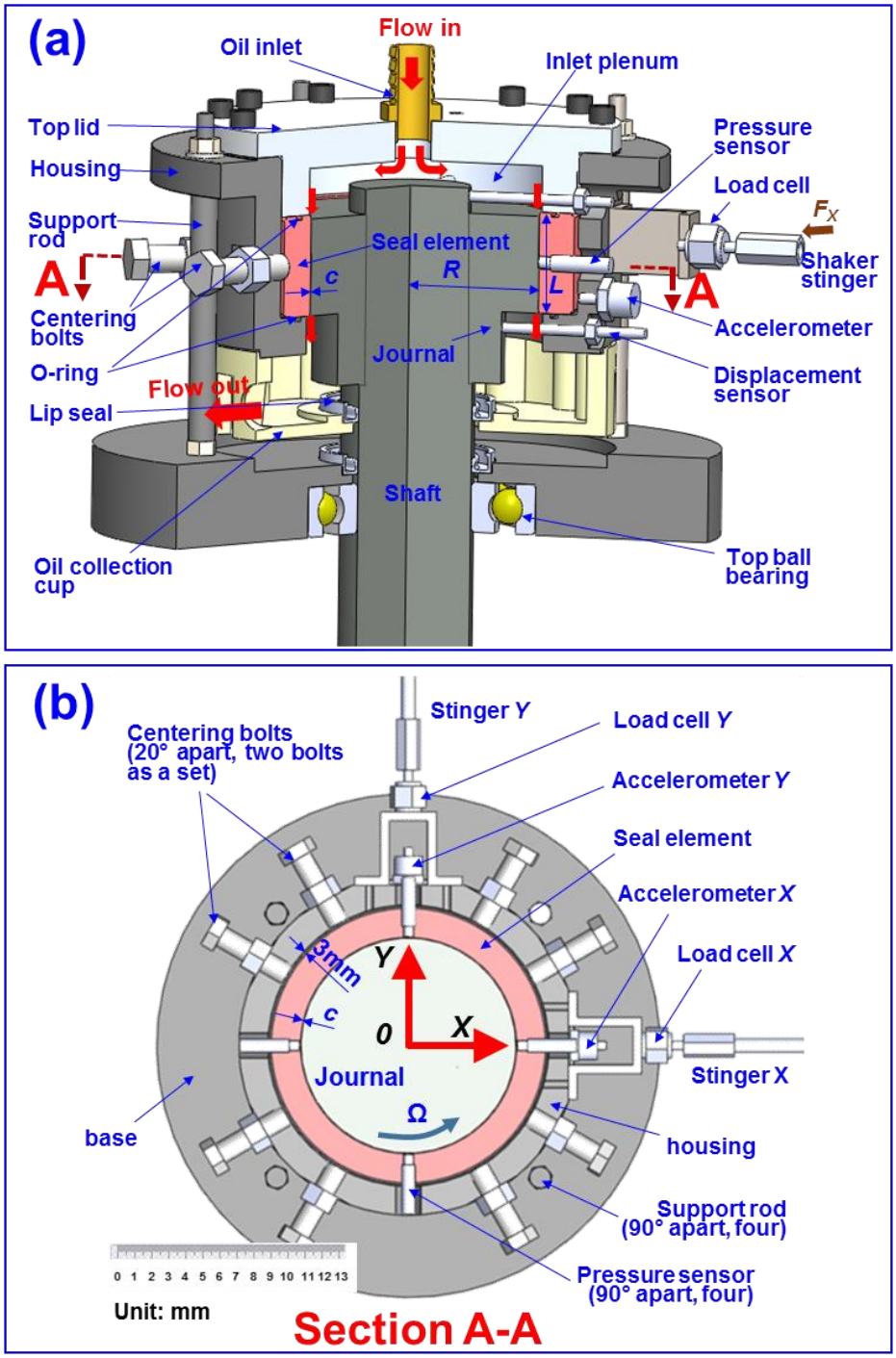

Fig. 4 (a) Cut view of test seal assembly with lubricant flow path, (b) section A-A with seal installed in housing (L = 46 mm, D = 127 mm, c_m = 0.191 mm).

The arrows in Fig. 4(a) depict the lubricant flow path. The fluids enters a plenum on top of the seal housing, and then flow through the seal annular clearance, to exit into an oil collection cup whose volume is ~3.5 times the size of the inlet plenum.

During the dynamic load tests, two load cells installed on the seal housing record the applied loads. Four eddy current sensors and two piezoelectric accelerometers record the ensuing seal housing motions and accelerations. A data acquisition system records voltage signals from sensors at a rate of 12.8 k samples/s and the acquisition time lasts typically 10.24 s. Other instrumentation includes static and dynamic pressure sensors, and flow meters for both the oil and air streams.

Figure 5 shows the fluids circulation system that consist of an air supply line drawing dry air from a large pressurized tank, and a gear pump and oil supply line that delivers ISO VG 10 oil at a constant volumetric flow rate. Two needle valves control the air volumetric flow rate and the oil flow rate. An air mass flow meter measures the air volumetric flow rate (Q_g) at a standard condition (20 ^{o}C and 1 bar(a)), and an oil turbine flow meter records the oil volumetric flow rate (Q_l). Both fluid streams merge into a sparger element with pore size of 2 μm to make an air in oil mixture. By regulating the needle valves, the system operator can make mixtures with any inlet gas volume fraction (GVF = 0 to 1) or liquid volume fraction (LVF = 0 to 1). The inlet GVF is defined as

$$\mathrm{GVF} = \frac{Q_{ga}(P_a / P_s)}{Q_l + Q_{ga}(P_a / P_s)} \tag{2}$$

where Q_{ga} is the air volumetric flow rate at a standard condition (1 bar(a), 20 °C), Q_l is the liquid volumetric flow rate, P_s is the supply pressure, and P_a is the ambient pressure. Accordingly, LVF = 1- GVF. The inlet gas mass fraction (GFM) is

$$\mathrm{GMF} = \frac{\mathrm{GVF} \cdot \rho_{ga} \cdot (P_s / P_a)}{\mathrm{GVF} \cdot \rho_{ga} \cdot (P_s / P_a) + (1 - \mathrm{GVF}) \cdot \rho_l} \tag{3}$$

After passing through the sparger, the mixture flows into the seal assembly to lubricate the seal element, to later exiting the seal housing. The flow stream then passes through a bubble eliminator where most of the air bubbles are removed. A gear pump returns the fluids to a large oil reservoir (tank). A division wall divides the oil tank into two parts, such that the mixture (with some remnant air) first returns into the right part of the tank to release the remnant gas. The liquid, having a higher density than the mixture, flows from

underneath the division wall to the left part of the tank. This arrangement ensures that the fluid in the left tank is pure oil. A feed pump, whose intake is placed ~ 175 mm below the oil level, delivers the oil into the oil supply line for making the air in oil mixture.

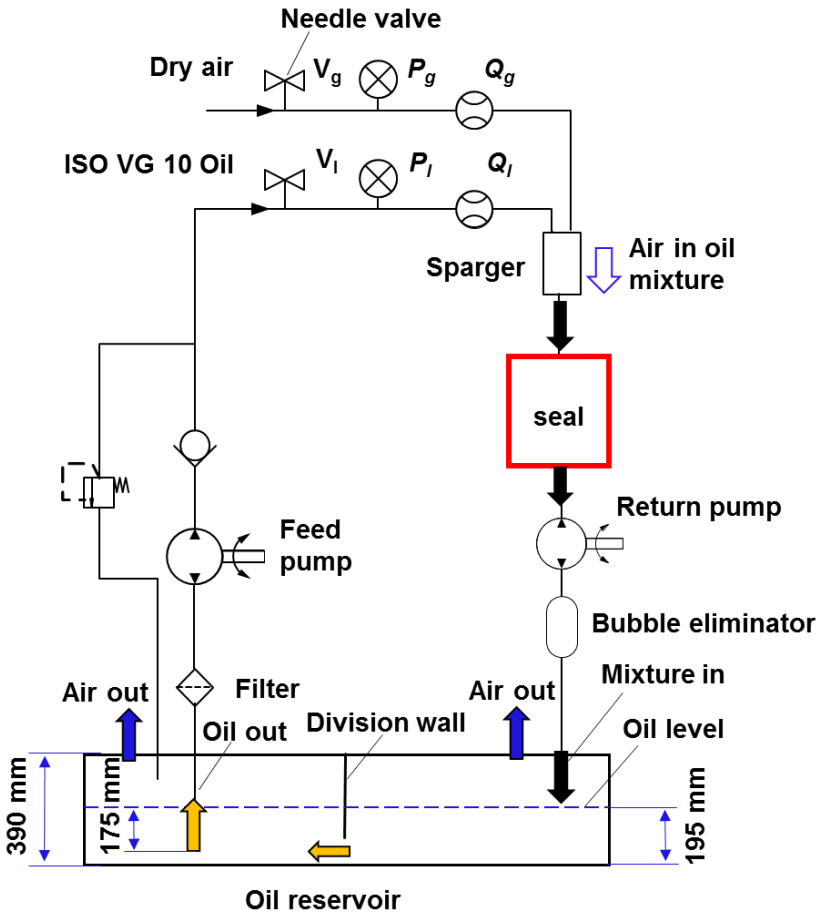

Fig. 5 Air and lubricant circulation flow systems.

Recorded flow rate for a three-wave annular seal and a plain cylindrical annular seal

The measured mixture mass flow through a seal is normalized with respect to the mass flow rate ($\dot{m}_{pl}$) obtained for a pure oil condition and at a null shaft speed, i.e., $\overline{\dot{m}}_m = (\dot{m}_m / \dot{m}_{pl})$. Figure 6(a) shows the measured (normalized) seal leakage versus inlet gas volume fraction (GVF) for the three-wave annular seal (open symbols) and the plain cylindrical annular seal with clearance c = 0.203 mm (solid symbols). The last results are taken from

Ref. [17].

In tests with a three-wave seal, the inlet GVF increases discretely from 0 to 1, the mixture inlet temperature T_{in} = 37 ± 1 °C, the supply pressure P_s = 2 bar(a), and the shaft speed N = 0 to 4 krpm (26.6 m/s). The tests for the plain seal are conducted at GVF = 0 to 0.97, supply pressure to 2 bar(a), shaft speed to 3.5 krpm (23.3 m/s), with the inlet mixture temperature at 34 ± 1 °C. The mass flow rate ($\dot{m}_{pl}$) for the three-wave seal operating with a pure oil at a null speed condition is 53 g/s. For similar conditions, the plain seal delivers $\dot{m}_{pl}$ = 40 g/s [17].

The normalized leakage $\dot{\bar{m}}_m$ for both the three-wave seal and the plain annular seal collapses into a single curve that decreases steadily in magnitude with an increase in inlet GVF. For operation with a static shaft (zero speed), $\dot{\bar{m}}_m$ for the three-wave seal is similar to that of a plain annular seal. However, for operation with a pure oil or a low GVF (GVF< 0.3) condition, the three-wave seal shows a significant increase in leakage (~1.35 times) as the shaft speed increases from 0 rpm to 4 krpm (ΩR = 26.7 m/s). During the test with the seal lubricated by a pure oil (GVF = 0) and the shaft spinning at a speed of 4 krpm, the temperature rise (ΔT) from the seal inlet plane to the outlet plane equals 7 °C. The viscosity for the ISO VG 10 oil decreases from 10.1 cP (at 37 °C) to 7.6 cP (at 44 °C). Thus, the decrease in viscosity (1.3 times) causes an increase in leakage (1.35 fold). The influence of shaft speed on the lubricant temperature rise (ΔT) decreases because the shaft drag power reduces with an increase in mixture GVF [17]. Indeed, when the inlet GVF increases to 0.4, ΔT is ~3.6 °C. Thus at an inlet GVF = 0.4, shaft speed has very little influence on $\dot{\bar{m}}_m$.

Predictions for seal leakage ($\dot{\bar{m}}_m$) based on a homogeneous flow model [10] match well with the test data over the range of 0.2 < GVF < 0.9 at zero shaft speed. Similar to observations detailed in Ref. [17], for operation with inlet GVF > 0.6, the seal leakage slightly decreases as the rotor speed increases, for example, $\dot{\bar{m}}_m$ (4 krpm) > $\dot{\bar{m}}_m$ (2.5 krpm). The homogeneous BFM does not predict this outcome.

A zoomed inset in Figure 6(b) shows that within the range 0.9 < GVF < 1, the prediction is slightly higher than the measured leakage. As shown in the inset, the predicted leakage equals to the measured leakage for operation with a pure air (GVF = 1).

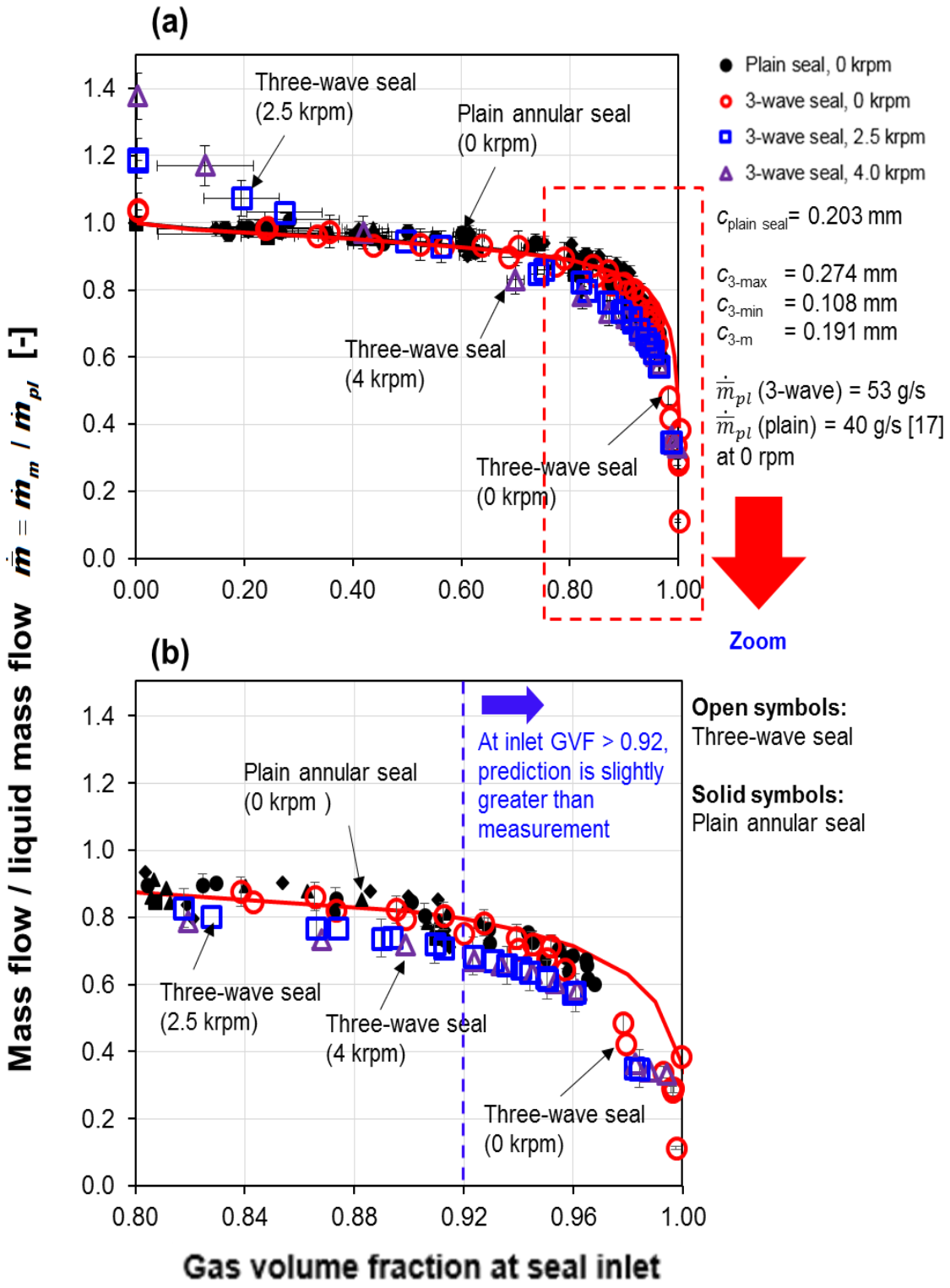

Fig. 6 (a) Three-wave annular seal and plain annular seal: Normalized leakage ($\dot{\bar{m}}_m$) vs. mixture inlet GVF. (b) Zoomed inset showing $\dot{\bar{m}}_m$ for 0.8 ≤ *GVF* ≤ 1. Supply pressure (P_s) 2 bar(a), discharge pressure (P_a) = 1 bar(a). Shaft speed N = 0 to 4 krpm (ΩR = 26.6 m/s).

Dynamic force coefficients for a three-wave seal

San Andrés and Lu [17] detail a procedure to identify frequency dependent force coefficients of a mechanical system. First, single frequency load tests performed on the *dry* system[2] without rotor speed deliver the structural stiffness K_S = 3.2 ±0.2 MN/m, system equivalent mass M_S = 14 ± 0.5 kg, and damping coefficient C_S = 0.38 ± 0.01 kN s/m. These coefficients are referred as "baseline" parameters.

Using a mechanical force gauge and a dial gauge, the estimated static stiffness K_S equals 3.4 MN/m and 3.2 MN/m along the *X* and *Y* directions. The mass of the seal structure plus the mass of the instruments attached to the seal housing is 13.9 kg as measured by a scale. The *dry* test system natural frequency ω_n = 78 Hz and its damping ratio $\xi_S \sim \dfrac{C_s}{2\sqrt{K_S M_S}}$ = 2.9%. An impact test reveals a natural frequency of 78.5 Hz.

Next, with the seal lubricated by either a pure oil or an air in oil mixture with a known inlet GVF, and the shaft spinning at speed *N*, one shaker applies an unidirectional load along the *X* direction to force the seal housing to displace with motion amplitude ($|X_X|$ and $|Y_X|$**)** at a frequency that ranges from 20 Hz to 150 Hz, in steps o 10 Hz. The other shaker (*Y* direction) is at rest. See Fig. 3(a) for depiction of the coordinates. The sensors record the force $\mathbf{F_{X(t)}} = [f_X = f_o e^{i\omega t}, f_Y = 0]^T$, the ensuing displacement $\mathbf{Z_{X(t)}} = [X_X, Y_X]^T$ with respect to the shaft, and the absolute seal housing acceleration $\mathbf{A_{X(t)}} = [a_{XX}, a_{YX}]^T$. Next, shaker *X* stops and shaker *Y* repeats the forced excitation. Similarly, the sensors record force $\mathbf{F_{Y(t)}} = [f_X = 0, f_Y = f_o e^{i\omega t}]^T$, the ensuing displacement $\mathbf{Z_{Y(t)}} = [X_Y, Y_Y]^T$ relative to the shaft, and the absolute seal housing acceleration $\mathbf{A_{Y(t)}} = [a_{XY}, a_{YY}]^T$. Note the amplitude of forced response at each test frequency is set at 10 μm, ~5 % of the seal mean clearance (c_m = 0.191 mm).

San Andrés [25] details the parameter identification procedure in the frequency domain. The procedure requires first to calculate the fundamental component of Fourier series for the recorded forces, accelerations and displacements at each test frequency, i.e., $f_X = f_o e^{i\omega t} \rightarrow X_X = \underline{X}_X e^{i(\omega t + \phi x)}$ and $Y_X = \underline{Y}_X e^{i(\omega t + \phi y)}$, where $i = \sqrt{-1}$ and ϕ_x , ϕ_y are phase angles. Next, assemble the matrices $\mathbf{F}_{(\omega)} = [\mathbf{F_{X(\omega)}} \mid \mathbf{F_{Y(\omega)}}]$, $\mathbf{A}_{(\omega)} = [\mathbf{A_{X(\omega)}} \mid \mathbf{A_{Y(\omega)}}]$, $\mathbf{Z}_{(\omega)} = [\mathbf{Z_{X(\omega)}} \mid \mathbf{Z_{Y(\omega)}}]$, which represent the applied forces, seal housing accelerations, and displacements at a

[2] A dry system denotes a test rig without oil or mixture supplied.

particular test frequency (say 20 Hz), respectively.

The test system has a complex dynamic stiffness matrix (**H**) defined as

$$\mathbf{H}(\omega)_{\text{system}} = [\mathbf{K} - \omega^2\mathbf{M} + i\omega\mathbf{C}] = [\mathbf{F}(\omega) - M_S\,\mathbf{A}(\omega)]\,\mathbf{Z}^{-1}(\omega) \quad (4)$$

Above M_S is the effective mass of the test rig housing and seal. Subtracting the *dry*[3] system force coefficients from the lubricated system yields the seal dynamic complex dynamic stiffness $\mathbf{H_{seal}} = \mathbf{H}_{\text{system}} - (\mathbf{K}_S + i\,\omega\,\mathbf{C}_S)$, thus

$$\mathbf{Re(H)}_{\text{seal}} = \text{Re}\mathbf{(H)}_{\text{system}} - \mathbf{K}_S \quad (5)$$

$$\mathbf{Ima(H)}_{\text{seal}} = \text{Ima}\mathbf{(H)}_{\text{system}} - \mathbf{C}_S\,\omega \quad (6)$$

where $\mathbf{K}_S = K_S\,\mathbf{I}$, $\mathbf{C}_S = C_S\,\mathbf{I}$, and **I** is a 2x2 identity matrix..

In a wet seal, the mixture is compressible due to the gas content, hence the force coefficients are frequency dependent [10]. Figure 7 shows the real and imaginary parts of the complex dynamic stiffnesses (H_{XX}, H_{YY}) vs. frequency (ω) for the three-wave seal lubricated with a pure oil (GVF = 0) and with a mixture with inlet gas volume fraction (GVF) varying from 0.2 to 0.9. The tests are conducted at an inlet pressure P_s = 2.5 bar(a), exit pressure P_a = 1 bar(a), a shaft speed equal to 3.5 krpm (58.3 Hz, ΩR = 23.3 m/s), and at an inlet mixture temperature T_{in} = 37 ± 1 °C. Table 2 lists the mixture leakage at the corresponding inlet GVF. Note the uncertainty for the real and imaginary parts of the complex dynamic stiffnesses is < 9.8 %

The graphs on the left of Figure 7 show Re(H_{XX}) and Re(H_{YY}). For operation with a pure liquid (GVF = 0), Re(H) decreases quadratically with whirl frequency (ω), evidencing a strong fluid inertia effect, i.e., Re(H_{XX}) → ($K_{XX} - \omega^2 M_{XX}$). A least square fit delivers the (oil only) seal force coefficients: K_{XX} = 1.1 ± 0.2 MN/m, K_{YY} = 1.7 ± 0.2 MN/m, C_{XX} = 31 ± 2 kN.s/m, C_{YY} = 32 ± 2 kN.s/m, M_{XX} = 5.1 ± 0.5 kg, and M_{YY} = 7.0 ± 0.5 kg. This result reveals a slight off centered seal. For operation with a minute eccentricity ratio (ε_X = -0.02, ε_Y = 0.03), the BFM model predicts K_{XX} = 1.1 MN/m, K_{YY} = 1.9 MN/m, C_{XX} = 30 kN.s/m, C_{YY} = 31 kN.s/m, M_{XX} = 6.1 kg, and M_{YY} = 6.3 kg. That is, the model delivers orthotropic force coefficients.

As the inlet GVF increases, the mixture shows a reduction in density (ρ_m/ρ_l) ~ (1-GVF); thus the fluid inertia effect in the seal reaction force reduces. In the current test with a GVF= 0.4 → 0.9, Re(H) shows a strong nonlinear frequency dependency. That is Re(H)

[3] The *dry* system parameters comprise the support structure stiffness (K_S) and a remnant damping (C_S).

first increases with frequency (ω) at ω < 80 Hz, and for ω> 80 Hz, Re(H) decreases again.

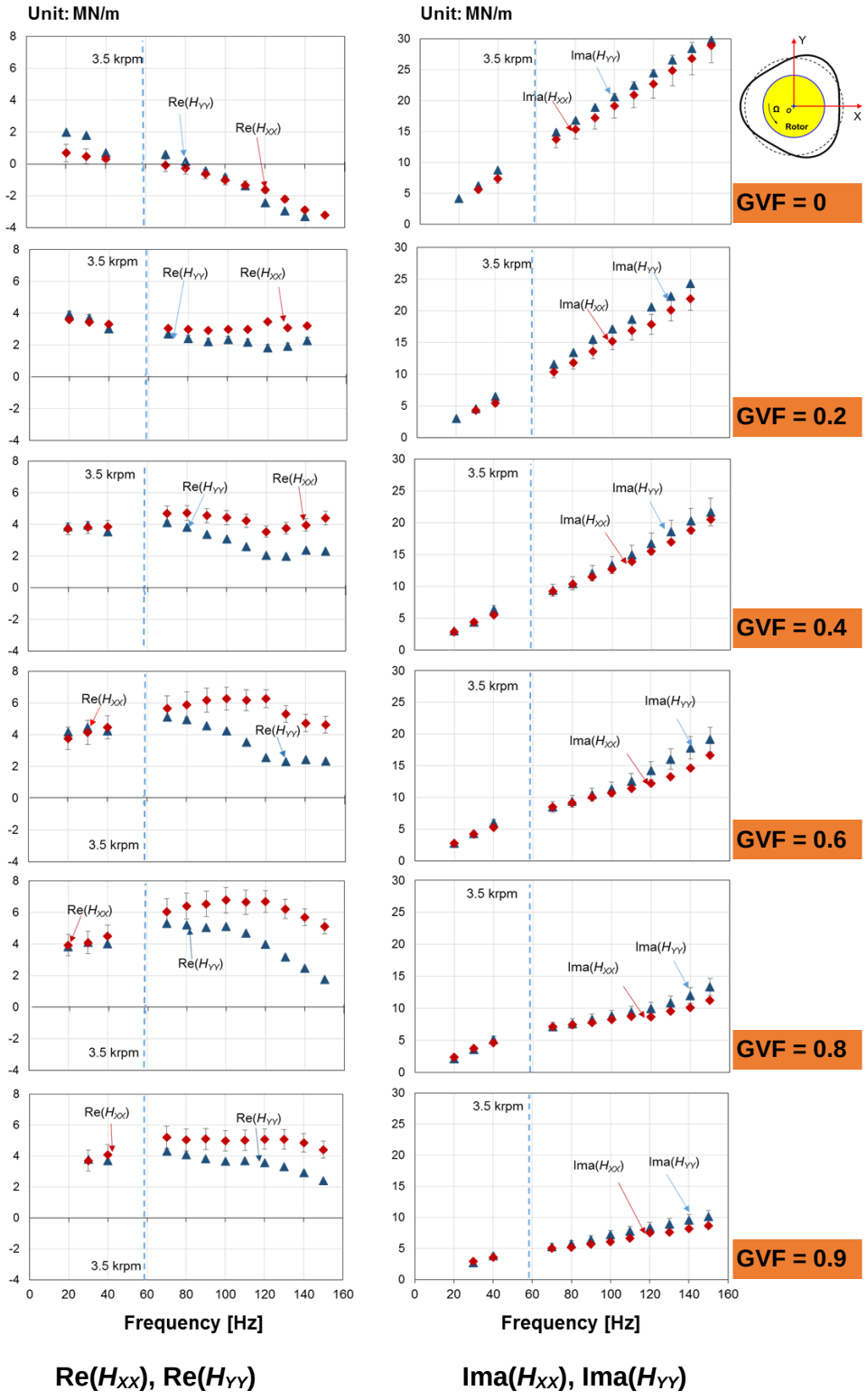

Fig. 7 Three-wave seal: Real and imaginary parts of direct complex dynamic stiffnesses H_{XX} and H_{YY} vs. frequency (ω). Inlet GVF = 0 to 0.9. Shaft speed = 3.5 krpm (ΩR = 23.3 m/s). Supply pressure (P_s) = 2.5 bar(a), discharge pressure (P_a) = 1 bar(a).

Table 2. Three-wave seal: mass flow rate versus inlet GVF. Shaft speed = 3.5 krpm. Supply pressure (P_s) = 2.5 bar(a), discharge pressure (P_a) = 1 bar(a).

Inlet GVF	0	0.2	0.4	0.6	0.8	0.9
Inlet GMF	0	$9.0\text{x}10^{-4}$	$2.3\text{x}10^{-3}$	$5.1\text{x}10^{-3}$	$1.4\ \text{x}10^{-2}$	$3.0\text{x}10^{-2}$
$\dot{m}_{\text{m}}$ (g/s)	100	83	75	64	57	49

Leakage uncertainty: $U_{\dot{m}_{\text{m}}} =$ 5 g/s

Recall that the seal is off centered with ε_X = -0.02 and ε_Y = 0.03. This will lead to an uneven clearance, thus more gas will enter the lobe where the clearance is relatively larger than other lobes to cause a reduction in the mixture density (ρ_m). Hence, $\text{Re}(H_{XX}) \neq \text{Re}(H_{YY})$. The predictions also deliver a similar outcome.

The graphs on the right of Figure 7 show Ima(H_{XX}) and Ima(H_{YY}) versus excitation frequency (ω). In general, for all the test conditions with inlet GVF = 0 → 0.9, Ima(H) increases linearly with frequency (ω), thus revealing a frequency independent damping coefficient, i.e., Ima(H) → (ωC). Note a continuous drop in the slope of Ima(H) with an increase in mixture GVF. A linear curve fit delivers the corresponding viscous damping coefficients (C_{XX}, C_{YY}) as listed in Table 3. Note that the seal damping coefficient for operation with GVF ≤ 0.4 is characterized by

$$C_m \simeq C_{pl} \cdot (1\text{-GVF}) \tag{7}$$

where $C_{pl} = ½ (C_{XX} + C_{YY})_{pl}$ is the average damping coefficient for a pure oil condition.

Note for GVF = 0.2 the mixture circumferential and axial Reynolds numbers are $\text{Re}_c = \frac{\rho_m V_C c}{\mu_m}$ 366, and $\text{Re}_z = \frac{\rho_m V_Z c}{\mu_m} = \frac{m_m}{\pi D \mu_m} =$ 31, thus the flow is laminar.

Recall that the current tests use unidirectional loads (X or Y) to procure the force coefficients. A circular whirl motion or a transient response to an impact load may lead to different damping coefficients for operation with a mixture [26].

Table 3. Three-wave seal damping coefficients (C) versus inlet GVF, Shaft speed = 3.5 krpm. Supply pressure (P_s) = 2.5 bar(a), discharge pressure (P_a) = 1 bar(a).

GVF	0	0.2	0.4	0.6	0.8	0.9
C_{XX} (kN.s/m)	31.0	24.4	21.1	17.2	12.4	9.8
C_{YY} (kN.s/m)	32.0	27.0	22.1	19.4	14.3	11.0
$C_{pl} \cdot (1\text{-GVF})$	31.5	25.2	18.9	12.6	6.3	3.2

Uncertainty: U_C = 9.8% of the identified damping coefficient

Figure 8 shows the real part of the cross-coupled complex dynamic stiffnesses (H_{XY}) and -(H_{YX}) vs. frequency (ω) for operation with a mixture with inlet GVF = 0 to 0.9. In tests with a pure oil (GVF = 0), Re(H_{XY}) and Re(H_{YX}) are frequency independent. At GVF = 0 a least square curve fit delivers K_{XY} = 4.7 ± 0.5 MN/m, and -K_{YX} = 5.7 ± 0.6 MN/m. The test data reveals the absence of a cross-coupled virtual mass (M_{XY} = M_{YX} = 0). The cross-coupled damping coefficients (C_{XY} = C_{YX}) are negligible compared with the direct terms thus they are not discussed here. Prediction shows K_{XY} = 4.8 MN/m, and -K_{YX} = 5.5 MN/m, and M_{XY} = M_{YX} = 0.

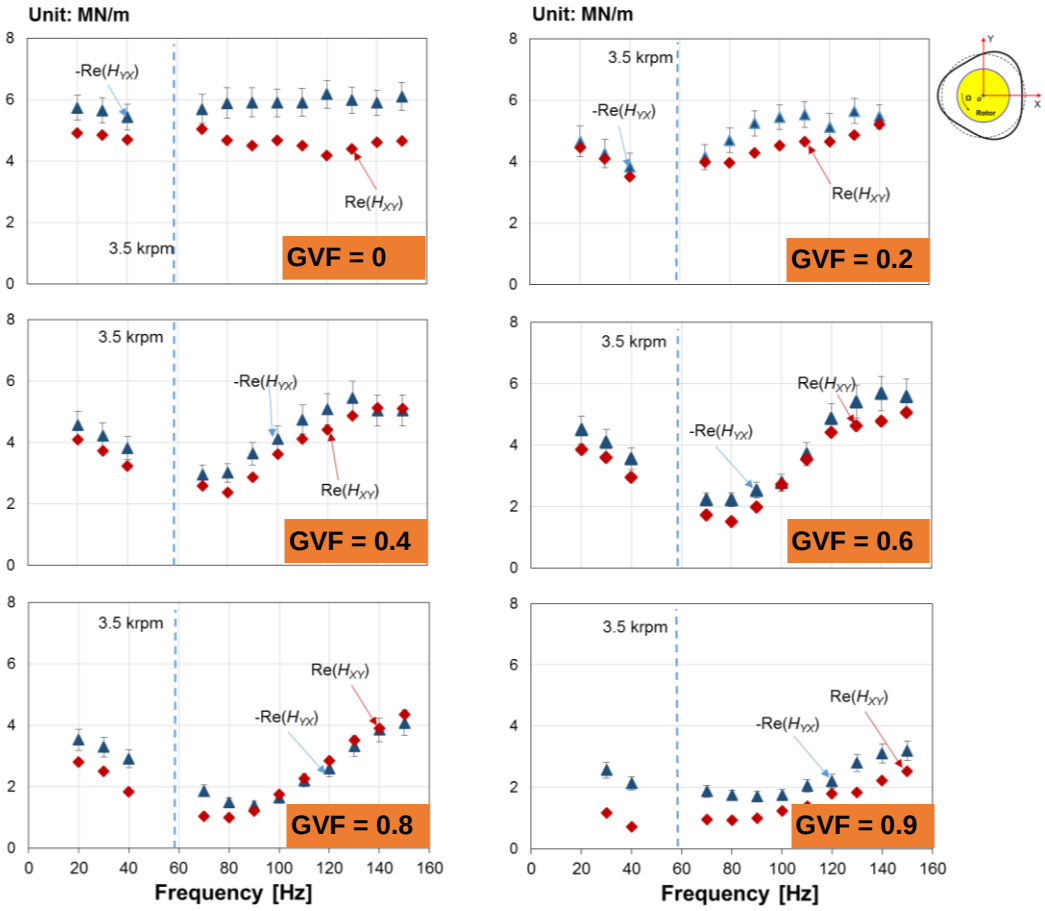

Fig. 8 Real part of cross-coupled complex dynamic stiffnesses H_{XY} and $-H_{YX}$ vs. excitation frequency (ω). Inlet GVF = 0 to 0.9. Shaft speed = 3.5 krpm (ΩR = 23.3 m/s). Supply pressure (P_s) = 2.5 bar(a), discharge pressure (P_a) = 1 bar(a).

For tests with the seal lubricated with a mixture with GVF = 0.2 → 0.9, both Re(H_{XY}) and -Re(H_{YX}) display a rapid decrease as frequency (ω) increases. The coefficients stop to decrease at $\omega = \Omega$ = 58.3 Hz for GVF = 0.2, or $\omega = \omega_n$ = 78 Hz for GVF = 0.4 to 0.9. After passing Ω or ω_n, the cross-coupled complex dynamic stiffnesses increase with frequency.

Note a continuous decrease in Re(H_{XY}) and -Re(H_{YX}) with an increase in mixture inlet GVF. Presently the cross-coupled coefficients are sizable in magnitude compared with the direct dynamic stiffnesses Re(H_{XX}) and Re(H_{YY}).

A key parameter to determine whether a seal is a stabilizing or destabilizing element in a rotor-bearing system is its effective damping coefficient, defined as [27, 28]

$$C_{XXeff} = C_{XX} - K_{XY}/\omega,\ C_{YYeff} = C_{YY} + K_{YX}/\omega \tag{8}$$

where $K_{XY} = Re(H_{XY})_{seal}$ and $K_{YX} = Re(H_{YX})_{seal}$ at $\omega > 0$. A positive effective damping coefficient is desirable as it produces a (tangential) force opposing the rotor whirl motion and thus promotes stability [27].

Figure 9 depicts the effective damping coefficient (C_{eff}) vs. frequency (ω) for the three-wave seal lubricated with a pure oil and a mixture with GVF = 0.2 → 0.9. At a low frequency $\omega \rightarrow 0$, $C_{effXX} \sim - K_{XY}/\omega$, whereas at $\omega >> 0$, $C_{effXX} \sim C_{XX}$. For operation with a pure oil, a three-wave seal exhibits a cross frequency[4] (ω_c) at 27.5 Hz (0.46X), which is slightly less than 50% of the shaft speed (0.5X). For operation with a mixture with inlet GVF = 0 → 0.8, the cross frequency does not show a significant reduction, i.e., ω_c = 0.46X → 0.43X. Note the calculated whirl frequency ratio (WFR) for a liquid seal is 0.47.

[4] A cross-frequency (ω_c) is the frequency at which C_{eff} changes from negative to positive.

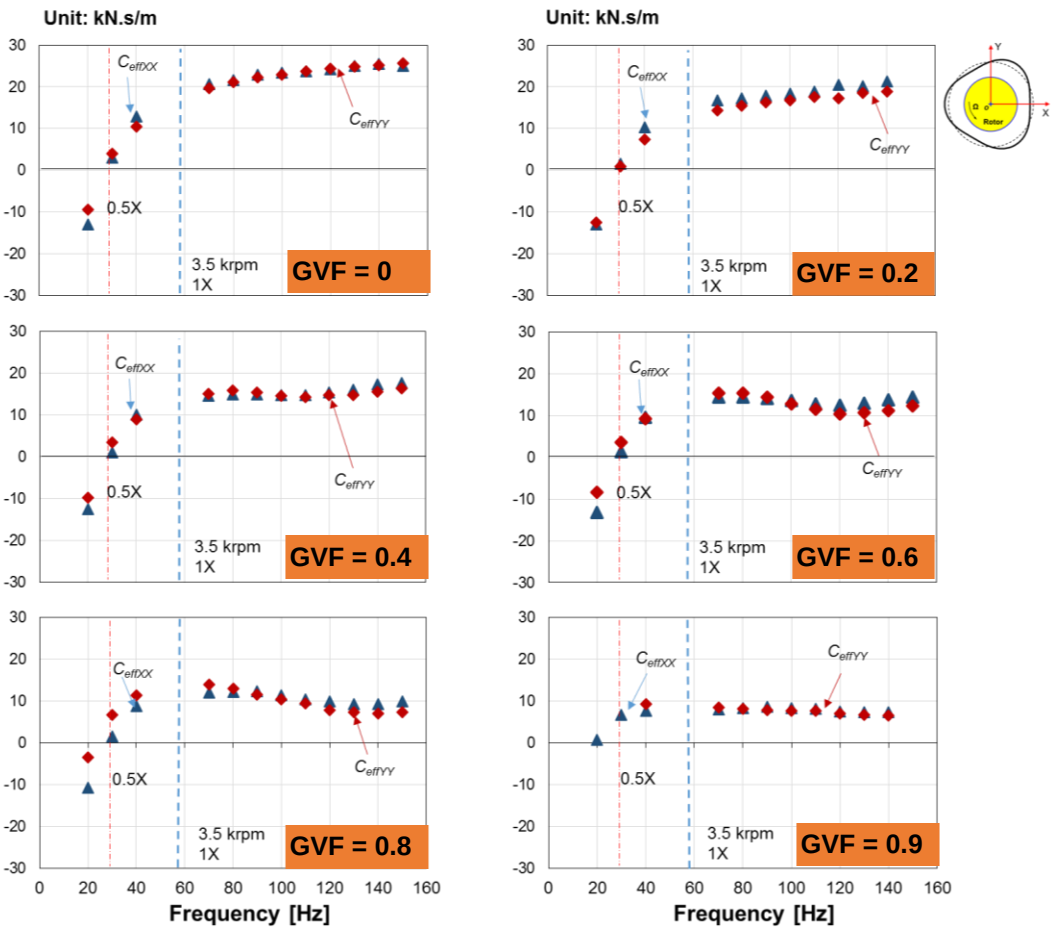

Fig. 9 Effective damping coefficients $C_{effXX} = (C_{XX} - K_{XY}/\omega)$, $C_{effYY} = (C_{XX} + K_{XY}/\omega)$ vs. frequency (ω). Inlet GVF = 0 to 0.9. Shaft speed = 3.5 krpm (ΩR = 23.3 m/s). Supply pressure (P_s) = 2.5 bar(a), discharge pressure (P_a) = 1 bar(a).

Comparison of dynamic force coefficients for a three-wave seal and two plain annular seals

Figures 10 to 12 show force coefficients for a three-wave seal annular seal, a plain annular seal (plain-seal-1, c = 0.203 mm) having the same mean clearance as the three-wave seal, and a plain annular seal (plain-seal-2, c = 0.274 mm) with a clearance equal to the maximum clearance of the three-wave seal (this case simulates a seal worn condition[5]). The specific operating conditions are inlet pressure P_s = 2.5 bar(a), inlet GVF = 0 to 0.9, and shaft speed = 3.5 krpm (ΩR = 23.3 m/s). The data is the arithmetic average along the X and Y directions, vertical error bars denote their standard deviation.

[5] Original wave seal machined to enlarge its clearance and remove waves.

Figure 10 shows the real and imaginary parts of the average complex direct stiffnesses (H_D) vs. frequency (ω). The graphs on the left depict H_D^R = ½ [Re(H_{XX})+Re(H_{YY})] . The three-wave seal shows a larger dynamic stiffness than plain-seal-1 because of its mechanical preload. A worn seal (plain-seal-2) with the largest clearance shows negligible stiffness at $\omega \rightarrow 0$. For operation with a pure liquid (GVF=0), Re(H) for both the three-wave seal and the two plain seals decreases quadratically with frequency ω, thus showing a strong fluid inertia effect Re(H) → (K-$\omega^2 M$). For operation with a mixture, the magnitude of Re(H) generally follows as: three-wave seal > plain-seal-1 > plain-seal-2.

The graphs on the right of Figure 10 show H_D^I = ½ [Ima(H_{XX})+Ima(H_{YY})]. For operation with a pure liquid (GVF = 0) or a mixture, H_D^I for both the three-wave seal and the two plain seals increases linearly with frequency ω. The three test seals show frequency independent damping coefficients, as cited Table 4. Not surprisingly, the damping coefficient (C) decreases continuously as the mixture inlet GVF increases from 0 to 0.9. The three-wave seal shows approximately 50% larger damping when compared with that of the plain-seal-1. The worn seal (plain-seal-2) shows less than 30% of the damping for the original three-wave seal.

Table 4. Direct damping coefficients for three annular seals versus inlet GVF

Inlet GVF		0	0.2	0.4	0.6	0.8	0.9
Damping C (kN.s/m)	Three-wave seal	31.5	25.7	21.6	18.3	13.4	10.4
	Plain-seal-1, c = 0.203 ± 0.004 mm	20.4	13.7	10.5	8.4	6.6	5.3
	Plain-seal-2, c = 0.274 ± 0.004 mm	9.6	9.4	8.3	6.5	3.3	1.9

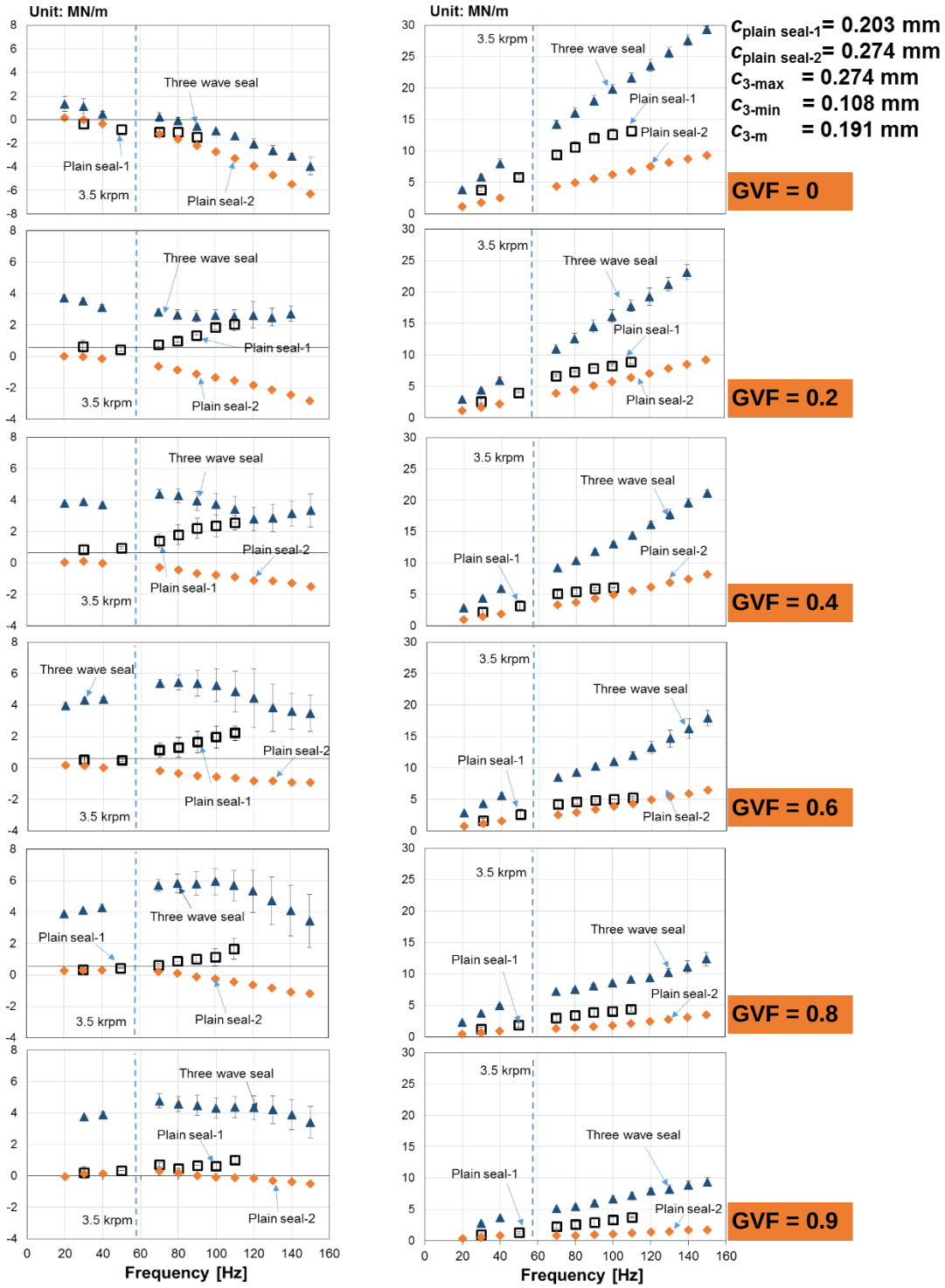

H_D^R = ½ [Re(H_{XX}) + Re(H_Y H_D^I = ½ [Ima(H_{XX}) + Ima(H_{YY})]

Fig. 10 Three-wave annular seal and two plain annular seals: real and imaginary parts of direct complex dynamic stiffnesses vs. frequency (ω). Inlet GVF = 0 to 0.9. Shaft speed = 3.5 krpm (ΩR = 23.3 m/s)**.** Supply pressure (P_s) = 2.5 bar(a), discharge pressure (P_a) = 1 bar(a).

Figure 11 shows the cross-coupled dynamic stiffnesses H_C^R = ½ [Re(H_{XY})-Re(H_{YX})] versus frequency (ω) for the three seals. The three-wave seal produces the largest cross coupled stiffness, followed by the plain-seal-1, and next by the worn seal (plain-seal-2). For all the three seals lubricated with a pure liquid (GVF = 0), H_C^R is frequency independent. However, a mixture whose inlet GVF = 0.2→0.9 produces frequency dependent cross coupled complex dynamic stiffnesses. Surprisingly, for operation with a mixture, the three seals show their smallest cross coupled stiffness at a frequency nearby the shaft running speed (58.3 Hz). No rationale is known for this peculiar outcome.

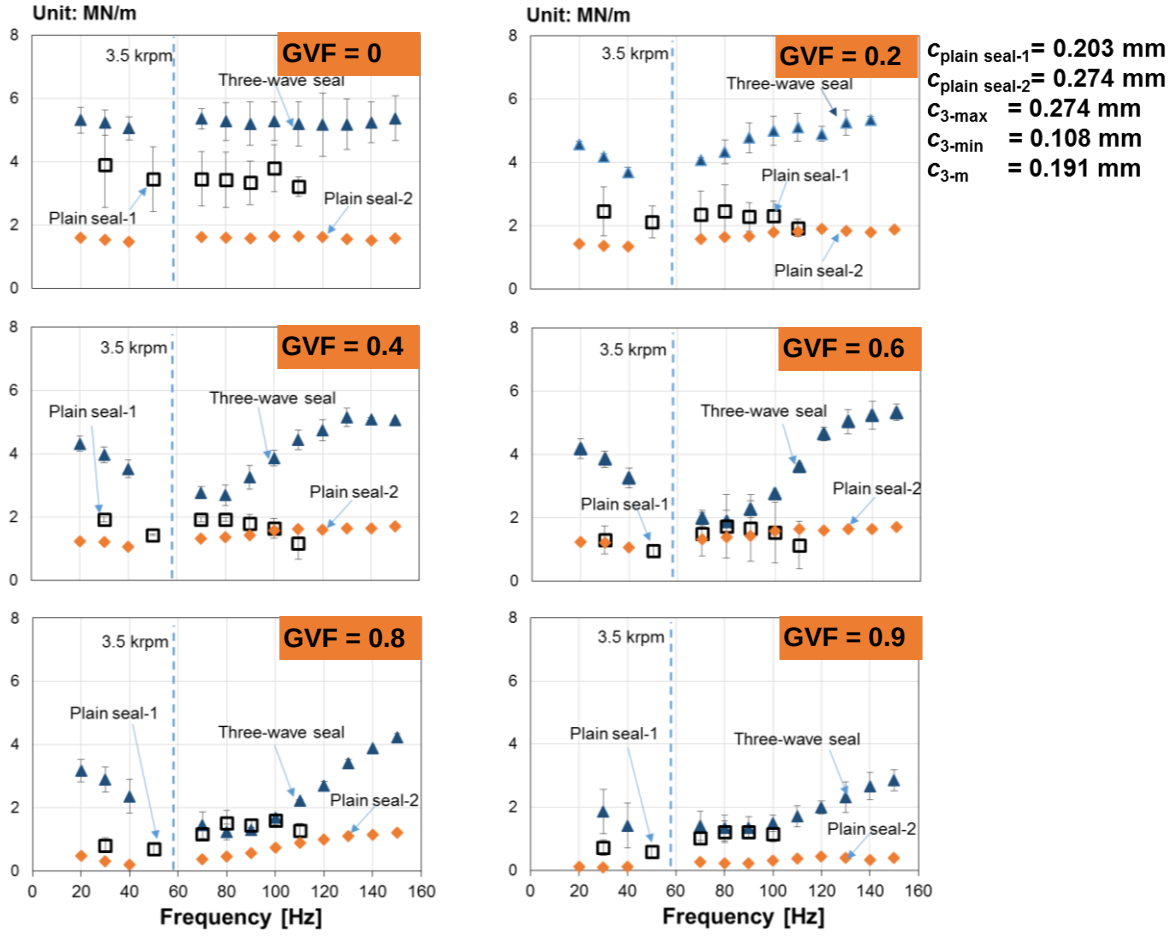

H_C^R = ½ [Re(H_{XY})-Re(H_{YX})]

Fig. 11 Three-wave annular seal and two plain annular seals: real parts of cross-coupled complex dynamic stiffnesses vs. frequency (ω). Inlet GVF = 0 to 0.9. Shaft speed = 3.5 krpm (ΩR = 23.3 m/s). Supply pressure (P_s) = 2.5 bar(a), discharge pressure (P_a) = 1 bar(a).

Figure 12 shows the effective damping coefficient $C_{eff} = ½ [C_{effXX}+C_{effYY})]$ vs. frequency (ω) for the three seals. The three-wave seal shows the greatest C_{eff} at $\omega > \omega_c$, where ω_c is the cross-over frequency. For operation with a mainly oil condition (GVF $\leq$ 0.4), C_{eff} increases with frequency for the three seals. However, for the three-wave seal operating with a mixture with GVF > 0.4, C_{eff} first increases with frequency until ω reaches 1X, C_{eff} then decreases as the frequency increases further. For the three seals, C_{eff} drops in magnitude with an increase in mixture GVF.

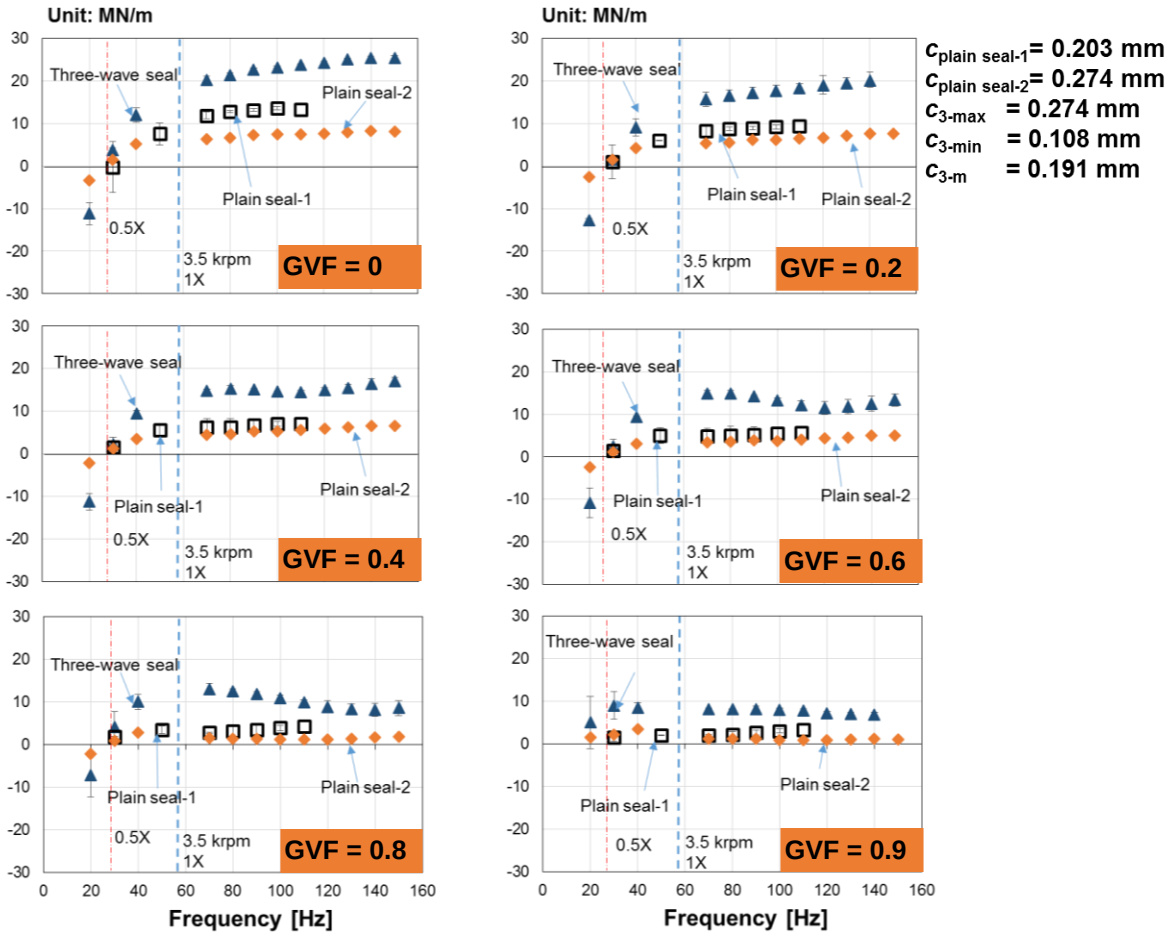

$$C_{eff} = ½ [C_{effXX} + C_{effYY}]$$

Fig. 12 Three-wave annular seal and two plain annular seals: effective damping coefficient vs. whirl frequency (ω). Inlet GVF = 0 to 0.9. Shaft speed = 3.5 krpm (ΩR = 23.3 m/s). Supply pressure (P_s) = 2.5 bar(a), discharge pressure (P_a) = 1 bar(a).

Predicted vs. experimental force coefficients for three-wave seal

Figure 13 (a) shows the predicted seal direct dynamic stiffness and experimental H_D^R = ½ [Re(H_{XX})+Re(H_{YY})] versus frequency (ω) as the inlet GVF increases, 0 → 0.9. The predictions are obtained for a journal eccentricity ratio ε_X = -0.02 and ε_Y = 0.03, as in the tests. For a pure oil condition (GVF = 0), both the predicted and measured dynamic stiffness show a strong downward curvature because the oil introduces a sizable added mass ($M \approx 6.1$ kg).

For operation with an air in oil mixture, the predicted H_D^R follows an upward trend (hardening) as frequency (ω) increases. The test data, except for the case with GVF = 0.2, first increases with frequency, to later decrease for ω > 80 Hz. Note that at a low frequency (20 Hz), both the predicted and experimental H_D^R show a quick increase as the inlet GVF increases from 0 (pure liquid) to 0.2.

Figure 13 (b) shows an expanded view for H_D^R at this particular low frequency (20 Hz). The dynamic stiffness increases rapidly from ~1.3 MN/m to ~4.2 MN/m (2.2 times larger) as the inlet GVF increases from 0 to 0.2. As the inlet GVF increases further from 0.2 to 0.9, the predicted H_D^R continuously reduces. On the other hand, the measured H_D^R remains relatively constant for operation with a GVF as large as 0.9. Recall that in Figure 10 the three-wave seal shows a prominent increase for H_D^R as the fluid changes from a pure oil (GVF = 0) to a mixture with inlet GVF = 0.2. However, plain seal-1 and plain seal-2 do not show a significant change in H_D^R. This phenomenon leads to a conclusion that the preload in the three-wave seal causes the increase in H_D^R for operation with a mixture and with a spinning shaft.

Figure 14 shows the predicted direct damping coefficient and experimentally identified C = ½ (C_{XX} +C_{YY}), where C = Ima(H/ω). Both the predicted and measured damping coefficients (C) decrease steadily with the amount of air in the mixture. For an oil seal (GVF = 0), the predicted C = 30 kN.s/m, and the test show C_{XX} ~ 32 kN.s/m. The damping coefficient (C) drops for GVF = 0 → 0.9. The predictions recreate the test data with accuracy for operation with inlet GVF = 0 and 0.2 only. Predictions under predict C by 50% for GVF = 0.4. The difference between the test results and the predictions increases with

GVF. The test results evidence larger damping coefficient than the predictions otherwise indicate.

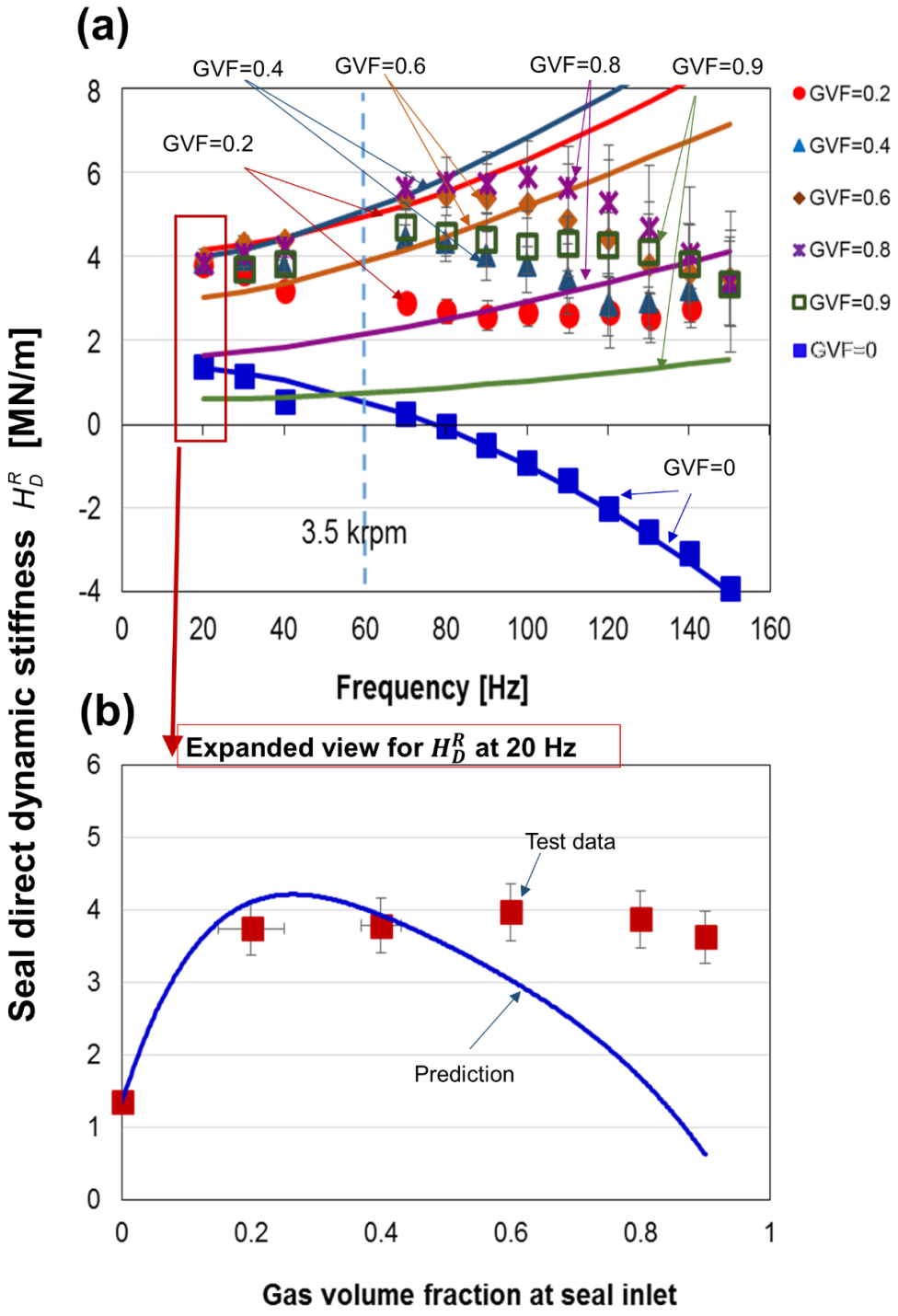

Fig. 13 (a) Three-wave seal direct dynamic stiffness: predicted and experimental H_D^R vs. frequency (ω). (b) Expanded graph showing H_D^R vs. inlet GVF at a low frequency 20 Hz. Shaft speed = 3.5 krpm (ΩR = 23.3 m/s). Supply pressure (P_s) = 2.5 bar(a), discharge pressure (P_a) = 1 bar(a).

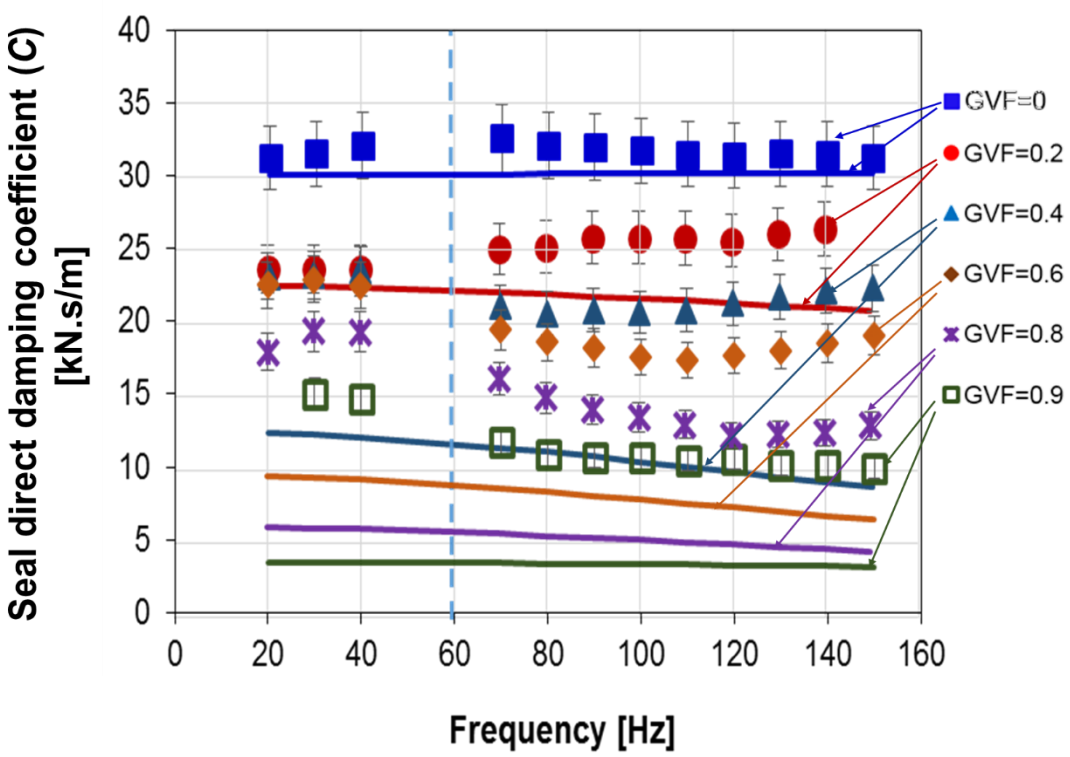

Fig. 14 Three-wave seal damping coefficient *C* = Ima(*H*/*ω*): predicted and experimental *C* vs. frequency (*ω*) and inlet GVF = 0 to 0.9. Shaft speed = 3.5 krpm (Ω*R* = 23.3 m/s). Supply pressure (P_s) = 2.5 bar(a), discharge pressure (P_a) = 1 bar(a).

Figure 15 shows the predicted cross-coupled dynamic stiffnesses and the test H_C^R = ½ [Re(H_{XY})-Re(H_{YX})]. For the liquid only seal (GVF = 0), both predictions and tests deliver a constant dynamic stiffness ~ 5.2 MN/m. For operation with a mixture (GVF > 0), the predicted H_C^R drops steadily with frequency. However, the experimental H_C^R first drops with frequency, yet to later increases when ω > 60 ~ 80 Hz. For operation with GVF = 0.2, H_C^R shows a dip at ~ 60 (Hz). As GVF ≥ 0.4, the frequency where the smallest magnitude of H_C^R occurs shifts from 60 Hz to 80 Hz (it approaches the structure natural frequency).

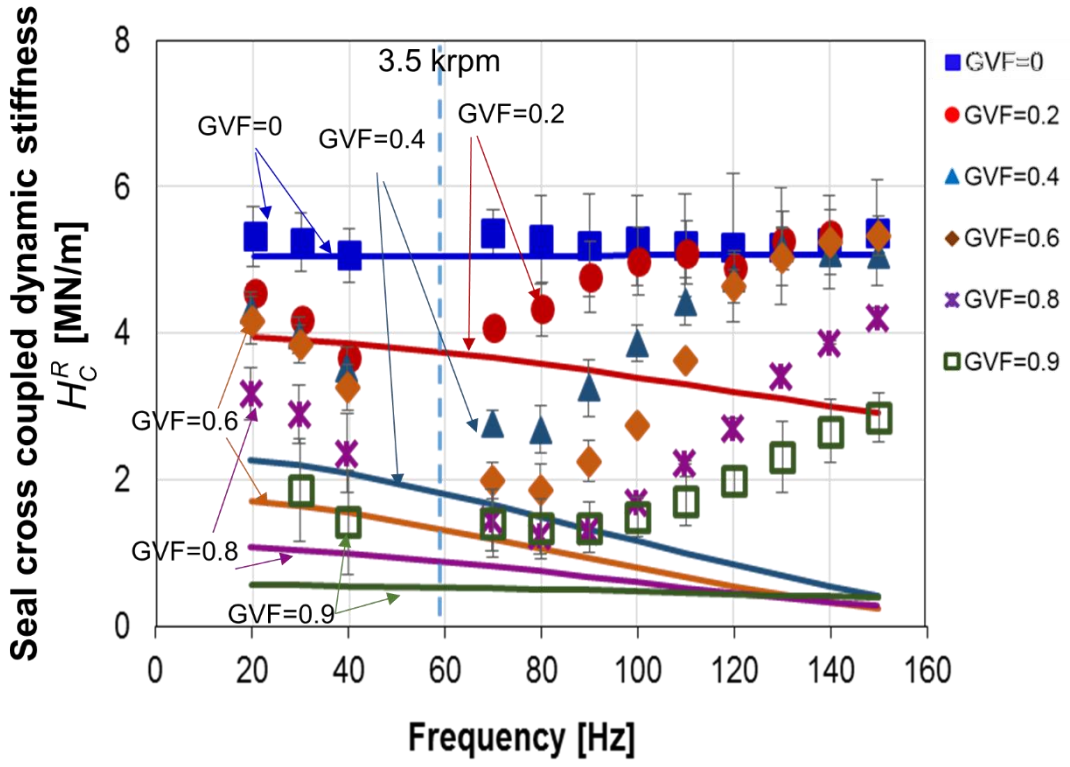

Fig. 15 Three-wave seal cross-coupled dynamic stiffness: predicted and experimental H_C^R vs. frequency (ω) and inlet GVF = 0 to 0.9. Shaft speed = 3.5 krpm (ΩR = 23.3 m/s). Supply pressure (P_s) = 2.5 bar(a), discharge pressure (P_a) = 1 bar(a).

Figure 16 depicts the predicted effective damping coefficients and the average of the test results C_{eff} = ½ (C_{XXeff} + C_{YYeff}). The prediction shows a steady increase in C_{eff} with frequency for operation with either a pure liquid or a mixture. On the other hand, C_{eff} decreases steadily with an increase in inlet GVF. The predictions match well the test results for operation with a pure oil and an inlet GVF = 0.2 condition. In addition, for the liquid seal only, C_{eff} = 0 at ω = 0.46 Ω = 27 Hz, which is slightly less than ½ Ω as expected for a laminar flow seal with a null inlet pre-swirl condition. Predictions deliver a cross-over frequency between 0.46 and 0.43 as GVF = 0 → 0.9.

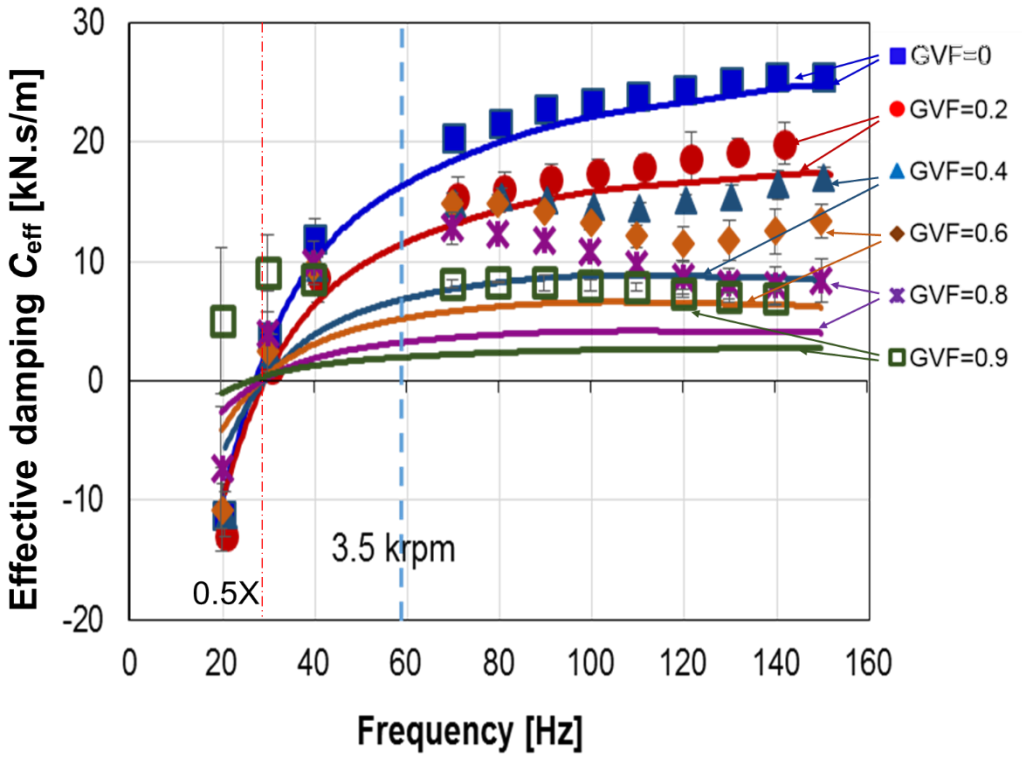

Fig. 16 Seal effective damping coefficient: predicted and experimental C_{eff} vs. frequency (ω) and inlet GVF = 0 to 0.9. Shaft speed = 3.5 krpm (58.3 Hz). Supply pressure (P_s) = 2.5 bar(a), discharge pressure (P_a) = 1 bar(a).

Conclusion

In a subsea environment, pumps must handle fluid mixtures with a GVF that spans a wide range (0 to 1). Similarly, compressors have to withstand efficient operation with a wet gas with a LVF up to 5%. Changes in LVF or GVF will affect the static and dynamic forced performance of seals which may cause SSVs in rotor bearing system [5]. Thus there is a need to study seal performance under a gas-liquid two-component condition.

This report extends the work in Ref. [17] and discusses the static and dynamic forced performance of a three-wave seal (L = 46 mm, D = 127 mm, c_m = 0.191 mm, ε_w = 0.43) operating at a speed of 3.5 krpm. An air in ISO VG 10 oil mixture with an inlet GVF varying discretely from 0 to 0.9 feeds the seal at a supply pressure (P_s) 2.5 bar(a) and exits the seal to ambient pressure P_a = 1 bar(a). The report also shows comparisons of force coefficients for three seals: a three-wave seal, a plain annular seal with a clearance equal to the mean clearance of the three-wave seal, and a plain annular seal with a clearance

equal to the maximum clearance of the three-wave seal to simulate a seal worn condition. The major findings for this work are:

(a) The measured mixture mass flow rate ($\dot{m}_m$) decreases continuously with an increase in inlet GVF. The normalized leakage ($\overline{\dot{m}}_m$) collapse into a single line.

(b) The three-wave seal lubricated with pure oil (GVF=0) shows frequency independent force coefficients where the direct stiffness K = 1.4 MN/m, cross coupled stiffness k = 5.2 MN/m, direct damping coefficient C = 31 kN.s/m, and inertia M = 6.1 kg.

(c) When lubricated with an air in oil mixture, the three-wave seal produces frequency dependent stiffnesses, direct and cross-coupled. Damping is not affected by frequency. The three-wave seal displays a prominent two-fold increase in Re(H) (at a low frequency 20 Hz) as the lubricant turns from a pure liquid (GVF=0) to a mixture with 20% gas (GVF=0.2).

(d) For the three wave seal, the cross frequency of the effective damping coefficient (C_{eff}) reduces slightly from 0.46X to 0.43X as the inlet GVF increases (GVF = 0 → 0.8).

(e) Among the three seals tested, the three-wave seal produces the largest direct stiffness, cross coupled stiffness, direct damping coefficients, effective stiffness, and effective damping coefficients

(f) Predictions of force coefficients from a homogeneous bulk flow model match well with test data for the three-wave seal for operation with a pure oil and a GVF = 0.2 condition. For operation with a mixture with GVF > 0.2, the predicted damping coefficient is generally 50% smaller than the test data. The BFM model does predict a rapid increase (200%) in direct dynamic stiffness as the inlet GVF increases from 0 to 0.2.

Currently, the BFM model does not consider the velocity difference between the two components. Future work will focus on modeling the effect of velocity slip between the gas and oil components to produce a sound prediction tool anchored with test data.

Nomenclature

c	Seal radial clearance [m]
c_{min}, c_{max}	Minimum and maximum radial clearance of three-wave seal [m]
c_m	½ (c_{min}+ c_{max}), mean clearance of three-wave seal [m]
$C_{i,j}$	Seal damping coefficients [N.s/m], $i, j = X, Y$
C_S	Structure damping coefficient [N/m],
D	$D = 2R$, Journal diameter [m]
e	Journal eccentricity [m]
e_w	$e_w = c_{max} - c_m$, Wave amplitude three-wave seal [m]
F_X, F_Y	External excitation force [N]
$H_{i,j}$	Seal complex dynamic stiffness [N.s/m], $i, j = X, Y$
H_D^R	½ [Re(H_{XX})+Re(H_{YY})]. Real part of seal direct complex dynamic stiffness [N/m]
H_D^I	½ [Ima(H_{XX})+Ima(H_{YY})]. Imaginary part of seal direct complex dynamic stiffness [N/m]
H_C^R	½ [Re(H_{XY})-Re(H_{YX})]. Real part of seal cross-coupled complex dynamic stiffness [N/m]
$K_{i,j}$	Seal stiffness coefficients[N/m], $i, j = X, Y$
K_S	Structure stiffness coefficient [N/m]
L	Seal length [mm]
$\dot{m}_l, \dot{m}_g$	Mass flow rate for pure liquid and pure gas [kg/s]
$\dot{m}_m$	$\dot{m}_m = \dot{m}_l + \dot{m}_g$, Mass flow rate of air in oil mixture [kg/s]
$\dot{m}_{pl}$	Mass flow rate for liquid only (GVF = 0) [kg/s]
$\bar{\dot{m}}_m$	$\bar{\dot{m}}_m = \dot{m}_m / \dot{m}_{pl}$, Normalized mass flow rate air in oil mixture [-]
$M_{i,j}$	Seal mass coefficients [N.s/m], $i, j = X, Y$
M_S	Structure mass coefficient [N/m],
N	Shaft rotational speed [rev/min]
n_w	Number of waves for wave seal [-]
P_a, P_s	Ambient pressure and supply pressure [Pa]
P_r	$P_r = P_s/P_a$, Pressure ratio [-]
Q_m	Volumetric flow rate for two-phase mixture [m^3/s]
Q_l , Q_g	Volumetric flow rate for pure liquid and pure gas [m^3/s]
R	R = ½ D, Journal radius [m]
Re$_c$	$\mathrm{Re}_c = \frac{\rho_m V_c c}{\mu_m}$, Circumferential flow Reynolds number [-]
Re$_z$	$\mathrm{Re}_z = \frac{\rho_m V_z c}{\mu_m} = \frac{\dot{m}_m}{\pi D \mu_m}$, Axial flow Reynolds number [-]
T	Temperature [K]
T_{in}	Seal inlet temperature [K]
V_c	V_c = ½ ΩR, ½ shaft surface speed [m/s]
V_z	V_z = $Q/\pi Dc$, Bulk flow axial velocity [m/s]

X,Y	Seal cartridge displacements [m]
$\varepsilon_{X,Y}$	$e_{X,Y}/c$, seal eccentricity ratio [-]
ε_w	$\varepsilon_w = e_w/c_m$, amplitude ratio of wave seal [-]
ξ	Test rig structural damping ratio [-]
μ_l, μ_{ga}	Liquid and gas viscosity at ambient pressure and T = 37 ºC [Pa.s]
μ_m	Two-phase flow effective viscosity [Pa.s]
ρ_l, ρ_{ga}	Liquid and gas density at ambient pressure and T = 37 ºC [kg/m^3]
ρ_m	Mixture or two-phase fluid density [kg/m^3]
ϕ	Phase angle between the applied force and the ensuing displacement [rad]
Ω	Shaft angular speed [rad/s]
ω	Excitation frequency [Hz]
ω_n	System natural frequency [Hz]

Matrices

A	Absolute acceleration vector [m/s^2]
C	System damping matrix, $\mathbf{C} = \mathbf{C_S} + \mathbf{C_{seal}}$ [N-s/m]
$\mathbf{C_S}$, $\mathbf{C_{seal}}$	Structure damping and seal damping matrices [N-s/m]
F	External excitation force vector [N]
H	$\mathbf{K}$- ω^2 $\mathbf{M}$ + i ω $\mathbf{C}$. System complex dynamic stiffness matrix [N/m]
I	Identity 2x2 matrix
K	System stiffness matrix, $\mathbf{K} = \mathbf{K_S} + \mathbf{K_{seal}}$ [N/m]
$\mathbf{K_S}$, $\mathbf{K_{seal}}$	Structure and seal stiffness matrices [N/m]
$\mathbf{M_S}$, $\mathbf{M_{seal}}$	Structure and seal mass matrices [kg]
Z	Seal cartridge displacement vector [m]

Subscripts

S	Structure
a	Ambient
inlet	Inlet plane of seal (z = 0)
m	Mixture or two component flow
g	Gas
l	Liquid

Abbreviations

GVF	Gas volume fraction
GMF	Gas mass fraction
LVF	Liquid volume fraction
SSV	Sub-synchronous vibration
BFM	Bulk flow model
WFR	Whirl frequency ratio

References

[1] Gong, H., Falcone, G., Teodoriu, C., Morrison, G. L., 2012, "Comparison of Multiphase Pumping Technologies for Subsea and Downhole Applications," Oil and Gas Facilities, **1**(01), pp. 36-46.

[2] 2016, "Next Gen Subsea Compressors to Reduce Size, Weight by 50%," *Turbomachinery International*, October 13, https://www.turbomachinerymag.com/advancing the-next-generation-in-subsea-compression-technology [access date]

[3] Dettwyler, M, Buche, D., Baumann, U., 2016, " Subsea Compression-Current Technology and its Use to Maximize Late Life Production," *Proceedings of the* 45th *Turbomachinery &* 32th *Pump Users Symposia*, Houston, TX, September 23-25

[4] Bertoneri, M., Wilcox, M., Toni, L. and Beck, G., 2014, "Development of Test Stand for Measuring Aerodynamic, Erosion, and Rotordynamic Performance of a Centrifugal Compressor under Wet Gas Conditions," ASME Paper GT2014-25349.

[5] Vannini, G., Bertoneri, M., Del Vescovo, G. and Wilcox, M., 2014, "Centrifugal Compressor Rotordynamics in Wet Gas Conditions," *Proceedings of the* 43th *Turbomachinery &* 30th *Pump Users Symposia*, Houston, TX, September 23-25.

[6] Iwatsubo, T., and Nishino, T., 1993, "An Experimental Study on the Static and Dynamic Characteristics of Pump Annular Seals," *Proceedings of the 7th Workshop on Rotordynamic Instability Problems in High Performance Turbomachinery*, College Station, TX, May 10–12, pp. 30-45. Available at http://turbolab.tamu.edu/resources/instability-workshops.

[7] Brennen, L., Bjorge, T., Gilarranz, J., 2005, "Performance evaluation of a Centrifugal Compressor Operating under Wet Gas Conditions," *Proceedings of the* 34th *Turbomachinery Symposium*, Houston, TX, USA.

[8] Vannini, G., Bertoneri, M., Nielsen, K.K., Ludiciani, P., Stronach, R., 2016, "Experimental Results and Computational Fluid Dynamics Simulations of Labyrinth and Pocket Damper Seals for Wet Gas Compression," ASME J. Eng. Gas Turb. Power, **138**, p. 052501.

[9] Ransom, D., Podesta, L., Camatti, M., Wilcox, M., Bertoneri M. Bigi, M., 2011, "Mechanical Performance of a Two Stage Centrifugal Compressor under Wet Gas Conditions," *Proceedings of the* 40th *Turbomachinery Symposium*, Houston, TX, Sept.

12-15.

[10] San Andrés, L., 2012, "Rotordynamic Force Coefficients of Bubbly Mixture Annular Pressure Seals," ASME J. Eng. Gas Turb. Power, **134**(2), p. 022503.

[11] Arghir, M., Zerarka, E., and Pieanu, G., 2011, "Rotordynamic Analysis of Textured Annular Seals with Multiphase (Bubbly) Flow," INCAS Bulletin, **3**(3), pp 3-13.

[12] San Andrés, L., Lu, X., and Liu, Q., 2016, "Measurements of Flow Rate and Force Coefficients in a Short-Length Annular Seal Supplied with a Liquid/Gas Mixture (Stationary Journal)," Tribol. Trans., **59** (4), pp. 758-767.

[13] Voigt, A.J., Mandrum-Polsen, C., Nielsen, K. K., Santos, I. F., 2016, "Design and Calibration of a Full Scale Active Magnetic Bearing Based Test Facility For Investigating Rotordynamic Properties of Turbomachinery Seals in Multiphase Flow," ASME J. Eng. Gas Turb. Power, **139**(5), p. 052505.

[14] Voigt, A.J., Iudiciani, P., Iudiciani, P., Nielsen, K. K., Santos, I. F., 2016, "CFD Applied for the Identification of Stiffness and Damping Properties for Smooth Annular Turbomachinery Seals in Multiphase Flow," ASME Paper No. GT2016-57905.

[15] Nelson, C.C., Nguyen, D.T., 1988, "Analysis of Eccentric Annular Incompressible Seals: Part 2—Effects of Eccentricity on Rotordynamic Coefficients," ASME J. Tribol., **110**, pp. 361 – 366.

[16] Childs, D.W., 2013, *Turbomachinery Rotordynamics with Case Studies*, Minter Spring Publishing, Wellborn, TX, Chap. 7. pp. 323-342.

[17] San Andrés, L., Lu, X., 2017, "Leakage, Drag Power and Rotordynamic Force Coefficients of an Air in Oil (Wet) Annular Seal," Proceedings of Turbo-Expo 2017, NC, USA. ASME Paper No. GT2017-63254 (Accepted for journal publication).

[18] Zhang, M., James E. Mclean Jr., Childs, D., 2017 "Experimental Study of the Static and Dynamic Characteristics of a Long Smooth Seal with Two-Phase, Mainly-Air Mixtrues," Proceedings of Turbo Expo 2017, NC, USA. Proceedings of Turbo-Expo 2017, NC, USA. ASME paper No. GT 2017-63988.

[19] Leader, M.E., Conner, K.J., Lucas, J.D., 2010, "Evaluating and Correcting Subsynchronous Vibration in Vertical Pumps," Proceedings of the 26th *International Pump Users Symposium,* September 2010, Texas A&M University, Houston, TX, USA.

[20] Dimofte, F., 1994, "Wave Journal Bearing with Compressible Lubricant – Part I: The Wave Bearing Concept and a Comparison To The Plain Circular Bearing," Tribol. Trans., **38**(1), pp. 153–160.

[21] Dimofte, F., 1995, "Wave Journal Bearing with Compressible Lubricant – Part II: A Comparison of the Wave Bearing with a Wave-Groove Bearing and a Lobe Bearing," Tribol. Trans., **38**(2), pp. 364–372.

[22] Dimofte, F., Hendricks, R.C., 2002, "Wave Journal Bearings under Dynamic Loads," NASA/TM-2002-211079. Available at: https://ntrs.nasa.gov/archive/nasa/casi.ntrs.nasa.gov/ 20020038212.pdf

[23] Ene, N.M., Dimofte, F., Keith Jr. T.G., 2008, "A Stability Analysis for a Hydrodynamic Three-Wave Journal Bearing," Trib. Int., **41**, pp. 434-442.

[24] Mitchell, L.D., and Elliott, K.B., 1984, "How to Design Stingers for Vibration Testing of Structures," Sound and Vibration. April, 1984, pp. 14-18.

[25] San Andrés, L., 2009, "Notes 14. Experimental Identification of Bearing Force Coefficients," Modern Hydrodynamic Lubrication Theory, Libraries Texas A&M University Repository, http://hdl.handle.net/1969.1/93254. [Access Mar 20, 2017].

[26] San Andrés, L., Diaz, S.E., and Rodriguez, L.E., 2001, "Sine Sweep Load vs. Impact Excitations and their Influence on the Damping Coefficients of a Bubbly Oil Squeeze Film Damper," Tribol. Trans., **44**(4), pp.692-698.

[27] Childs, D.W., 1993, *Turbomachinery Rotordynamics: Phenomena, Modeling, and Analysis*, John Wiley & Sons, Inc. NY.

[28] Kleynhans, G.F., Childs, D.W., 1997, "The Acoustic Influence of Cell Depth on the Rotordynamic Characteristics of Smooth-Rotor/Honeycomb-Stator Annular Gas Seals," ASME J. Eng. Gas Turb. Power, **119,** pp. 949-956.